

Adversarial Transform Particle Filters

Chengxin Gong¹, Wei Lin², Cheng Zhang^{3,*}

Abstract

The particle filter (PF) and the ensemble Kalman filter (EnKF) are widely used for approximate inference in state-space models. From a Bayesian perspective, these algorithms represent the prior by an ensemble of particles and update it to the posterior with new observations over time. However, the PF often suffers from weight degeneracy in high-dimensional settings, whereas the EnKF relies on linear Gaussian assumptions that can introduce significant approximation errors. In this paper, we propose the Adversarial Transform Particle Filter (ATPF), a novel filtering framework that combines the strengths of the PF and the EnKF through adversarial learning. Specifically, importance sampling is used to ensure statistical consistency as in the PF, while adversarially learned transformations, such as neural networks, allow accurate posterior matching for nonlinear and non-Gaussian systems. In addition, we incorporate kernel methods to ease optimization and leverage regularization techniques based on optimal transport for better statistical properties and numerical stability. We provide theoretical guarantees, including generalization bounds for both the analysis and forecast steps of ATPF. Extensive experiments across various nonlinear and non-Gaussian scenarios demonstrate the effectiveness and practical advantages of our method.

Keywords: Adversarial learning; Data assimilation; Ensemble Kalman filter; Particle filter; State-space models.

1 Introduction

Data assimilation plays a critical role in fields such as meteorology (Rabier, 2005), oceanography (Bertino et al., 2003), and geophysics (Fletcher, 2022). In these fields, state-space models (SSMs) are often employed to describe the evolution dynamics of the system state, and the relationship of the latent states to observed data. The goal of data assimilation is to obtain an estimate of the true latent states of the system and the associated uncertainty of that estimate. At each time step, the learning and inference process consists of two sequential alternating phases: analysis and forecast. During the analysis phase, current observations are used to update prior knowledge of the latent state, resulting in a posterior distribution that provides a more accurate estimate of the current state. In the forecast phase, the posterior distribution is propagated forward using the evolution dynamics to predict the distribution and likely value of the next state. While numerous methods exist to perform these two steps (Evensen, 1994; Gordon et al., 1993; Anderson, 2001; Lei & Bickel, 2011), the forecast phase generally relies on predefined evolution dynamics. Therefore, in this paper we focus on improving the analysis

¹School of Mathematical Sciences and Center for Statistical Science, Peking University, Beijing, 100871, China. Email: gongchengxin@pku.edu.cn

²School of Mathematical Sciences and Center for Statistical Science, Peking University, Beijing, 100871, China. Email: weilin@math.pku.edu.cn

³School of Mathematical Sciences and Center for Statistical Science, Peking University, Beijing, 100871, China. Email: chengzhang@math.pku.edu.cn

*Corresponding author

step to efficiently transform prior particles into posterior ones for more accurate latent state estimation. There is an enormous statistics and engineering literature on state estimation for data assimilation. For linear, Gaussian models, the Kalman filter (Kalman, 1960) provides an efficient closed-form solution for posterior state estimation given the observations. For more general SSMs with nonlinear, non-Gaussian models, Markov chain Monte Carlo (MCMC) methods have been developed (Carlin et al., 1992; Shephard & Pitt, 1997; Gamerman, 1998). While these methods are effective, they struggle to scale to high-dimensional states in view of the rapidly growing computational cost (typically cubically) as the state dimension increases. An alternative approach for general SSMs is sequential Monte Carlo, also known as the particle filter (PF; Gordon et al. (1993)). The PF approximate the state distribution using a weighted set of samples or *particles*, which are propagated forward over time according to the state evolution dynamics and updated with new observations via reweighting or resampling, typically using importance sampling. Although PFs are exact in the limit of infinite particles, they tend to suffer from weight degeneracy (i.e., all weights but one become essentially zero), especially in high dimensions (Snyder et al., 2008). While various PF variants have been proposed to alleviate this issue (Arulampalam et al., 2002; Nakano et al., 2007; Xiong et al., 2006; Murphy & Russell, 2001), scaling PFs to high-dimensional problems remains a significant challenge. Instead of adjusting particle weights, one can update the particles directly to approximate the posterior using an appropriate transformation. For example, the ensemble Kalman filter (EnKF; Evensen (1994)) updates the ensemble of particles using a linear “shift” that approximates the best linear update, assuming a linear Gaussian model. While this approach enhances particle diversity, it sacrifices statistical consistency in the context of nonlinear and non-Gaussian models. Furthermore, in high-dimensional scenarios, the EnKF requires additional techniques to avoid rank deficiency and underestimation of forecast-error covariance matrices (Sun et al., 2024). Three main methods are typically used: dimension localization (e.g., Hunt et al. (2007); Montemerlo et al. (2003)), covariance tapering (e.g., Anderson (2007); Furrer et al. (2006)) and inflation (e.g., Evensen (2003); Lei & Bickel (2011)). These approaches assume that correlations decrease rapidly with spatial distance, implying that the covariance matrix should be sparse. Besides these, numerous EnKF variants, such as the ensemble transform Kalman filter (ETKF; Bishop et al. (2001)) and the ensemble adjustment Kalman filter (EAKF; Anderson (2001)), have been developed to improve approximation accuracy and reduce computational burden.

In this paper, we propose the adversarial transform particle filter (ATPF), a new framework for data assimilation in SSMs that combines the statistical consistency of the PF with the particle diversity of the EnKF through the lens of adversarial learning. In the field of generative models, adversarial learning has proven successful, as exemplified by generative adversarial networks (GANs; Goodfellow et al. (2014)) and further Wasserstein GANs (W-GANs; Arjovsky et al. (2017)), which can effectively approximate complex target data distributions. From a statistical perspective, W-GANs distinguish between two distributions, P and Q , using the maximum mean discrepancy (MMD), also known as the integral probability metric (IPM) or adversarial loss. Specifically, a set of test functions, denoted by \mathcal{F}_D , acts as a discriminator to measure the dissimilarity between P and Q , which leads to the MMD defined as follows:

$$\text{MMD}(P||Q) = \sup_{f \in \mathcal{F}_D} |\mathbb{E}_{x \sim P} f(x) - \mathbb{E}_{x \sim Q} f(x)|. \quad (1)$$

Similar to the EnKF, we aim to learn a transformation function to update prior particles toward the posterior. As shown in equation 1, only the expectations of the test functions under P and Q are needed. By leveraging importance sampling, as in PFs, we can estimate these expectations under the posterior distribution and train the transformation function by minimizing the MMD between the pushforward

of the prior and the posterior. Unlike the EnKF, this adversarial framework allows us to match arbitrary posterior distributions, making it particularly well-suited for nonlinear and non-Gaussian models. Moreover, the approach inherits key advantages from both the PF and the EnKF. On one hand, the transformation formulation and adversarial loss in equation 1 mitigates particle collapse. On the other hand, the posterior expectations from PFs ensure statistical consistency in the estimates.

The remainder of the paper is organized as follows. In Section 2, we provide a brief introduction to state-space models (SSMs) and review existing filtering methods. Our proposed method is presented in detail in Section 3, followed by an exploration of its theoretical properties in Section 4. Section 5 presents the experimental results that validate our method. We conclude the paper and offer further discussions in Section 6. All proofs are provided in Appendix A.

2 State-Space Models and Ensemble Methods

2.1 State-Space Models

We begin with a brief introduction to state-space models (SSMs), which describe the temporal evolution of the latent state and how it relates to the observations. The SSM is defined as

$$\begin{aligned}x_t &= \mathcal{M}_{t-1}(x_{t-1}) + \eta_t, \\y_t &= \mathcal{H}_t(x_t) + \varepsilon_t,\end{aligned}\tag{2}$$

where $x_t, \eta_t \in \mathbb{R}^{d_{x_t}}$ denote the latent state and the evolution noise, $y_t, \varepsilon_t \in \mathbb{R}^{d_{y_t}}$ denote the observed data and the observation noise, the evolution operator $\mathcal{M}_{t-1} : \mathbb{R}^{d_{x_{t-1}}} \mapsto \mathbb{R}^{d_{x_t}}$ and the observation operator $\mathcal{H}_t : \mathbb{R}^{d_{x_t}} \mapsto \mathbb{R}^{d_{y_t}}$ are both measurable functions, for each time $t = 1, \dots, T$. Without loss of generality, we set $\mathbb{E}\eta_t = \mathbb{E}\varepsilon_t = 0$. In the data assimilation problem, it is commonly assumed that (1) the analytical forms of $\mathcal{M}_{t-1}, \mathcal{H}_t$ are fully known; (2) η_t, ε_t are mutually independent for all $t = 1, \dots, T$; and (3) densities p_{η_t} and p_{ε_t} are simple and straightforward to sample from. At each time t , all filtering methods perform two sequential steps: the analysis step and the forecast step. The goal of the analysis step is to transform the prior $p_t(x_t) := p(x_t|y_{1:t-1})$ into the posterior $q_t(x_t) := p(x_t|y_{1:t})$, while the forecast step aims to estimate the prior $p_{t+1}(x_{t+1}) := p(x_{t+1}|y_{1:t})$ for the next time step.

The optimal transformation in the analysis step is naturally induced by Bayes' rule, which gives the posterior

$$q_t(x_t) = \frac{p_t(x_t)p_{\varepsilon_t}(y_t - \mathcal{H}_t(x_t))}{\int p_t(x)p_{\varepsilon_t}(y_t - \mathcal{H}_t(x))dx}.\tag{3}$$

However, a closed-form solution to this equation is only tractable in a few special cases, such as when $\mathcal{M}_t, \mathcal{H}_t$ are linear functions and η_t and ε_t are Gaussian variables, or when x_t is discrete. In more general scenarios, ensemble filtering methods are often employed to approximate the solution, where $p_t(x_t), q_t(x_t)$ are represented by an ensemble of particles and the updating rules operate directly on these particles. Two essential methods for this are the PF and the EnKF, which we introduce next.

2.2 Particle Filter

Particle filters (PFs) (Gordon et al., 1993) update the prior particles by recalculating their weights according to the associated likelihood of the observed data using self-normalized importance sampling (SNIS; Kong (1992)). At time t , given the prior particles $\{x_t^1, \dots, x_t^n\}$ and the corresponding weights $\{w_t^1, \dots, w_t^n\}$, the vanilla PF algorithm works as follows:

PF Step 1: Compute the likelihood $l_t^i = p_{\varepsilon_t}(y_t - \mathcal{H}_t(x_t^i))$ for $i = 1, \dots, n$.

PF Step 2: Update the weights $\tilde{w}_{t+1}^i = w_{t+1}^i l_t^i$ for $i = 1, \dots, n$ and renormalize $w_{t+1}^i \propto \tilde{w}_{t+1}^i$ such that $\sum_{i=1}^n w_{t+1}^i = 1$.

PF Step 3: Sample $x_{t+1}^i = \mathcal{M}_t(x_t^i) + \eta_{t+1}^i$ with $\eta_{t+1}^i \stackrel{\text{i.i.d.}}{\sim} p_{\eta_{t+1}}$ for $i = 1, \dots, n$ to obtain forecast particles $\{x_{t+1}^1, \dots, x_{t+1}^n\}$ with weights $\{w_{t+1}^1, \dots, w_{t+1}^n\}$.

The PF method is asymptotically consistent since the distribution induced by the weighted particles converge weakly to the true posterior as the number of particles goes to infinity (Künsch, 2005). When the effective sample size $\text{ESS} := \frac{1}{\sum_{i=1}^n (w_t^i)^2}$ becomes relatively small, which is likely to occur in high-dimensional settings, an additional resampling step can be introduced between steps 2 and 3 to mitigate weight degeneracy:

PF Step 2a: Resample from the ensemble $\{x_t^1, \dots, x_t^n\}$ with weights $\{w_{t+1}^1, \dots, w_{t+1}^n\}$ for n times, that is, sample from the distribution $\sum_{i=1}^n w_{t+1}^i \delta(x - x_t^i)$ for n times. Then set $w_{t+1}^i \equiv \frac{1}{n}$ for $i = 1, \dots, n$.

As mentioned in Section 1, the resampling step may fail to improve particle diversity when the evolution law is deterministic, i.e., $\mathbb{P}(\eta_t = 0) = 1$ for all $t = 1, \dots, T$, as identical particles will remain identical as time evolves. To address this issue, the regularized PF method (Musso et al., 2001; Arulampalam et al., 2002) adopts the kernel smoothing trick. Let $m(\cdot)$ denote a kernel density function satisfying $\int m(x)dx = 1$. After step 2 or step 2a, we can take the following step:

PF Step 2b: Sample from the kernelized mixture distribution $\sum_{i=1}^n w_{t+1}^i m(x - x_t^i)$ for n times. Then set $w_{t+1}^i \equiv \frac{1}{n}$ for $i = 1, \dots, n$.

2.3 Ensemble Kalman Filter

For each time t , assume a linear Gaussian state-space model

$$x_t = M_t x_{t-1} + \eta_t, \quad (4)$$

$$y_t = H_t x_t + \varepsilon_t, \quad (5)$$

where $M_t \in \mathbb{R}^{d_{x_t} \times d_{x_{t-1}}}$, $\eta_t \sim \mathcal{N}_{d_{x_t}}(0, Q_t)$, $H_t \in \mathbb{R}^{d_{y_t} \times d_{x_t}}$, $\varepsilon_t \sim \mathcal{N}_{d_{y_t}}(0, R_t)$. When the prior distribution is Gaussian, the posterior remains Gaussian and explicit update formulas for the mean and variance parameters can be derived. This is the well-known Kalman filter (Kalman, 1960; Kim et al., 2018). In high dimensions, however, maintaining and propagating full covariance matrices becomes computationally expensive and memory demanding. To address these issues, Evensen (1994) proposed the EnKF which represents the state distribution using an ensemble of particles. This ensemble is propagated forward through time and updated as new observations become available. Given the prior forecast ensemble $\{x_t^1, \dots, x_t^n\}$ and the perturbed observation y_t , the EnKF proceeds as follows:

EnKF Step 1: Estimate the covariance of x_t by the sample covariance: $P_t := \widehat{\text{Cov}}(x_t, x_t) = \frac{1}{n-1} \sum_{i=1}^n (x_t^i - \bar{x}_t)(x_t^i - \bar{x}_t)^T$ where $\bar{x}_t = \frac{1}{n} \sum_{i=1}^n x_t^i$ is the forecast mean.

EnKF Step 2: Estimate the Kalman gain as $K_t := P_t H_t^T (H_t P_t H_t^T + R_t)^{-1}$.

EnKF Step 3: For each $i = 1, \dots, n$, sample $\varepsilon_t^i \stackrel{\text{i.i.d.}}{\sim} \mathcal{N}(0, R_t)$ and generate the corresponding pseudo-observation y_t^i as $y_t^i = H_t x_t^i + \varepsilon_t^i$.

EnKF Step 4: For each $i = 1, \dots, n$, update the particle x_t^i as

$$x_t^i \leftarrow x_t^i + K_t (y_t - y_t^i). \quad (6)$$

EnKF Step 5: For each $i = 1, \dots, n$, sample $x_{t+1}^i = \mathcal{M}_t(x_t^i) + \eta_{t+1}^i$ with $\eta_{t+1}^i \stackrel{\text{i.i.d.}}{\sim} p_{\eta_{t+1}}$.

In high dimensions, techniques such as covariance inflation or covariance tapering can be incorporated between steps 4 and 5, while localization can be applied during step 4. These strategies, which will be elaborated in Appendix C, enhance the performance of the EnKF in complex settings. However, the linear transformations used in the EnKF are often suboptimal for nonlinear or non-Gaussian models. While some non-Gaussian EnKF approaches have been proposed (Anderson, 2010; Lei & Bickel, 2011), they still exhibit poor performance for certain classes of measurement distributions (Katzfuss et al., 2020).

3 Adversarial Transform Particle Filter

In this section, we present the adversarial transform particle filter (ATPF), a novel adversarial learning framework for data assimilation that integrates the particle diversity of the EnKF with the statistical consistency of the PF. The key motivations for ATPF are: (1) extending the linear update equation in the EnKF (i.e., equation 6) and similar methods to more flexible, general transformations; (2) replacing the moment-matching criteria in the nonlinear ensemble adjustment filter (NLEAF; Lei & Bickel (2011)) with a maximum mean discrepancy (MMD) objective, which offers greater effectiveness for distributional matching.

Let \mathcal{G}_t and \mathcal{F}_D be two pre-specified function spaces, where \mathcal{G}_t represents the collection of transformation functions and \mathcal{F}_D represents the collection of test functions. For a given time t , let $G_t \in \mathcal{G}_t$ denote the transformation function, which takes the prior particles as inputs and outputs the estimated posterior samples. Let \hat{P}_t and P_t be the estimated and the ground truth prior, respectively, where P_t may be estimated via PFs or Markov chain Monte Carlo (MCMC) methods. Similarly, let \hat{Q}_t and Q_t be the corresponding estimated and true posterior distributions. Specifically, $\hat{Q}_t = G_{t\#}\hat{P}_t$ (“#” denotes the pushforward operator) and Q_t can be estimated with a reweighted version of P_t via importance sampling. Our goal is to ensure that \hat{Q}_t closely approximates the true posterior Q_t under the adversarial loss equation 1. This leads to the oracle objective of minimizing the MMD:

$$G_t = \arg \min_{G_t \in \mathcal{G}_t} \sup_{f \in \mathcal{F}_D} \left| \mathbb{E}_{x \sim \hat{Q}_t} f(x) - \mathbb{E}_{x' \sim Q_t} f(x') \right| = \arg \min_{G_t \in \mathcal{G}_t} \sup_{f \in \mathcal{F}_D} \left| \mathbb{E}_{x \sim \hat{P}_t} f(G_t(x)) - \mathbb{E}_{x' \sim P_t} b_t(x') f(x') \right|, \quad (7)$$

where $b_t(\cdot)$ is a weighting function defined as:

$$b_t(x') = \frac{dQ_t}{dP_t} = \frac{p_{\varepsilon_t}(y_t - \mathcal{H}_t(x'))}{\int p_t(x) p_{\varepsilon_t}(y_t - \mathcal{H}_t(x)) dx}. \quad (8)$$

Since computing the normalizing constant $\int p_t(x) p_{\varepsilon_t}(y_t - \mathcal{H}_t(x)) dx$ is intractable, we adopt the self-normalized importance sampling (SNIS; Hesterberg (1988)) instead. By leveraging the empirical distributions of the priors, the transformation function \hat{G}_t can be learned by minimizing the empirical MMD:

$$\hat{G}_t = \arg \min_{G_t \in \mathcal{G}_t} \widehat{\text{MMD}}(\hat{Q}_t \| Q_t) = \arg \min_{G_t \in \mathcal{G}_t} \sup_{f \in \mathcal{F}_D} \left| \frac{1}{N_1} \sum_{i=1}^{N_1} f(G_t(x_t^i)) - \sum_{j=1}^{N_2} \frac{w_t(x_t^j)}{\sum_{j=1}^{N_2} w_t(x_t^j)} f(x_t^j) \right|, \quad (9)$$

where $w_t(x) = w_{t-1}(x) p_{\varepsilon_t}(y_t - \mathcal{H}_t(x))$, $x_t^i \stackrel{\text{i.i.d.}}{\sim} \hat{P}_t$ for $i = 1, \dots, N_1$, and $x_t^j \stackrel{\text{i.i.d.}}{\sim} P_t$ for $j = 1, \dots, N_2$. Since the estimator given by SNIS is biased, N_2 is often chosen to be larger than N_1 for better estimation of the posterior expectation.

Once \hat{G}_t is learned, we can immediately obtain the posterior ensemble $\{\hat{G}_t(x_i)\}_{i=1}^{N_1}$. Then we can

Algorithm 1 The adversarial transform particle filter algorithm for SSMs

Input: $y_{1:T}, \mathcal{M}_{1:T}, \mathcal{H}_{1:T}, Q_{1:T}, R_{1:T}, \alpha, \tau$
Output: $\{x_1^i\}_{i=1}^{N_1}, \dots, \{x_T^i\}_{i=1}^{N_1}$

- 1: Sample $\{x_0^i\}_{i=1}^{N_1}, \{x_0^j\}_{j=1}^{N_2}$ from the prior and set $w_j \equiv \frac{1}{N_2}$ for $j = 1, \dots, N_2$;
 - 2: **for** $t = 1, \dots, T$ **do**
 - 3: Update $w_j, j = 1, \dots, N_2$ for $\{x_t^j\}_{j=1}^{N_2}$ according to PF Steps 1 and 2;
 - 4: Train G_t with learning rate α until convergence or reach the iteration limit τ ;
 - 5: Update the particle x_t^i as $x_t^i \leftarrow G_t(x_t^i)$ for $i = 1, \dots, N_1$;
 - 6: **if** $t \neq T$ **then**
 - 7: Resample from $\{x_t^j\}_{j=1}^{N_2}$ according to their corresponding weights $\{w_j\}_{j=1}^{N_2}$;
 - 8: Execute the inflation step equation 43 for $\{x_t^i\}_{i=1}^{N_1}$ and $\{x_t^j\}_{j=1}^{N_2}$, respectively;
 - 9: Execute the forecast step (EnKF Step 5) for all particles.
 - 10: **end if**
 - 11: **end for**
-

execute the forecast step (e.g., EnKF step 5) and obtain the estimate for the next latent state. The detailed procedure is outlined in Algorithm 1.

3.1 The MMD in Reproducing Kernel Hilbert Spaces

The MMD training objective equation 9 shares a similar form with that of GANs, which suggests that it may inherit challenges such as instability and difficulty in training when G_t and f are optimized alternately. It turns out that we can eliminate the inner optimization of f by restricting the test functions \mathcal{F}_D to the unit ball of a reproducing kernel Hilbert space (RKHS).

Proposition 1 (Kernel MMD, Smola et al. (2006)). *Let $K(\cdot, \cdot)$ denote the reproducing kernel. Under the RKHS constraint $\mathcal{F}_D = \{f : \|f\|_{\mathcal{H}} \leq 1\}$, the squared MMD takes the explicit form*

$$\text{MMD}^2(P\|Q) = \mathbb{E}_{x, x' \sim P} K(x, x') - 2\mathbb{E}_{x \sim P, y \sim Q} K(x, y) + \mathbb{E}_{y, y' \sim Q} K(y, y'). \quad (10)$$

The above proposition demonstrates that using the kernel method, the challenging bi-level optimization can be reduced to a more standard and tractable problem:

$$\begin{aligned} G_t &= \arg \min_{G_t \in \mathcal{G}_t} \sup_{f \in \mathcal{F}_D} \left| \mathbb{E}_{x \sim \hat{Q}_t} f(x) - \mathbb{E}_{y \sim Q_t} f(y) \right| = \arg \min_{G_t \in \mathcal{G}_t} \text{MMD}^2(\hat{Q}_t \| Q_t) \\ &= \arg \min_{G_t \in \mathcal{G}_t} \left\{ \mathbb{E}_{x, x' \sim \hat{P}_t} K(G_t(x), G_t(x')) - 2\mathbb{E}_{x \sim \hat{P}_t, y \sim Q_t} K(G_t(x), y) + \mathbb{E}_{y \sim Q_t, y' \sim Q_t} K(y, y') \right\}. \end{aligned} \quad (11)$$

We can use the V-statistics (Akritas, 1986; Serfling, 2009) to estimate the first term, and use the SNIS to estimate the second term. The last term can be omitted as it is independent of G_t . With this simplification, we can learn G_t by minimizing the empirical kernel MMD

$$\hat{G}_t := \arg \min_{G_t \in \mathcal{G}_t} \frac{1}{N_1^2} \sum_{i=1}^{N_1} \sum_{j=1}^{N_1} K(G_t(x_i), G_t(x_j)) - \frac{2}{N_1} \sum_{i=1}^{N_1} \sum_{j=1}^{N_2} \frac{w_t(x'_j)}{\sum_{j=1}^{N_2} w_t(x'_j)} K(G_t(x_i), x'_j). \quad (12)$$

We refer to this approach as the Kernel Adversarial Transform Particle Filter (KATPF).

3.2 Optimal Transport Regularization

When updating the prior to the posterior in SSMs, an optimal transport (OT, Reich (2013)) approach has been employed to identify a transformation that minimizes the expected distance between the two

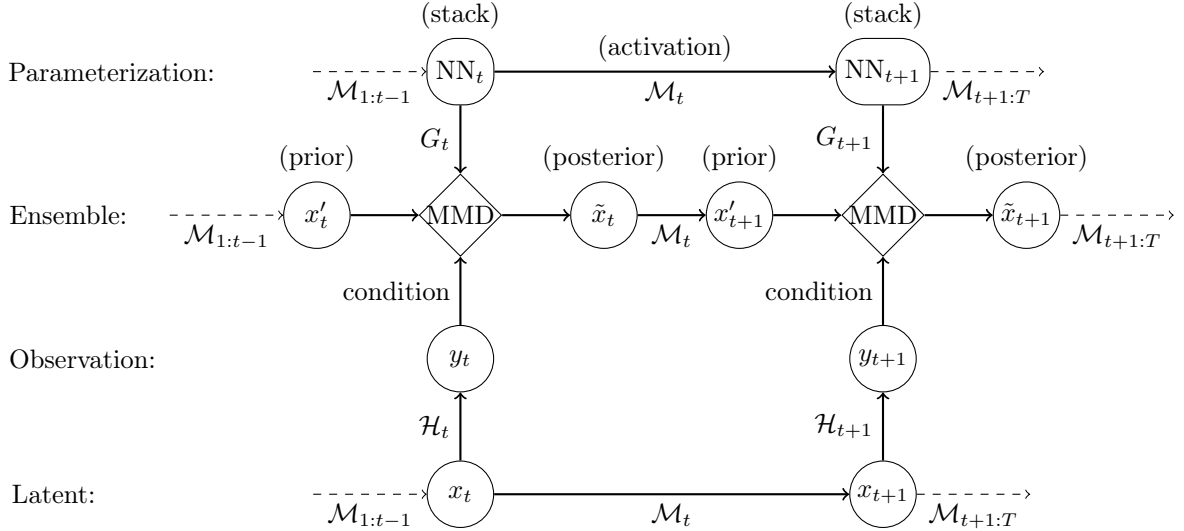


Figure 1: Our parameterization methods and flow chart of filtering for SSMs.

distributions and ensure statistical consistency for infinite samples (Reich, 2013). Likewise, we can incorporate OT to regularize the transformation as

$$G_t := \arg \min_{G_t \in \mathcal{G}_t} \text{MMD}^2(\hat{Q}_t \| Q_t) + \lambda_t W_2^2(\hat{Q}_t, P_t), \quad (13)$$

where W_2 is the Wasserstein-2 distance. Similar optimization objectives can also be found in other works (Jordan et al., 1998; Fan et al., 2021). Intuitively, when the space of the test functions is relatively limited and insufficient (which induces a weak MMD metric), the regularization provided by the W_2 distance can help maintain numerical stability during iterative updates without compromising statistical consistency (Reich, 2013). Furthermore, it can prevent our ATPF particles from overfitting and being too similar to the PF particles, which are known to exhibit several issues such as weight degeneracy and sample impoverishment (Poterjoy, 2016; Snyder et al., 2008).

In practice, we may use the coupling induced by the transformation to form a surrogate (upper bound) of the W_2 distance, which leads to the following regularized optimization

$$\tilde{G}_t := \arg \min_{G_t \in \mathcal{G}_t} \text{MMD}^2(G_{t\#} P_t \| Q_t) + \lambda_t \mathbb{E}_{x \sim P_t} \|G_t(x) - x\|_2^2. \quad (14)$$

Lemma A.1 in Xu et al. (2024) reveals the equivalence between equation 13 and equation 14. Furthermore, the surrogate can be estimated as

$$\mathbb{E}_{x \sim P_t} \|G_t(x) - x\|_2^2 \approx \frac{1}{N_1} \sum_{i=1}^{N_1} \|G_t(x_i) - x_i\|_2^2. \quad (15)$$

3.3 Neural Network Parameterization and Joint Optimization

The rich family of test functions used in ATPF provides better distributional matching capability than the NLEAF methods that only use the first and second moments. Moreover, compared to the EnKF that uses linear transformations, we use more flexible nonlinear transformations based on neural networks for more accurate posterior estimation.

While it is natural to train these transformations sequentially, we can also train them jointly by

minimizing the sum of the MMD and W_2 regularization terms across all observation times:

$$\hat{G}_{1:T} = \arg \min_{(G_1, \dots, G_T) \in \mathcal{G}_1 \times \dots \times \mathcal{G}_T} \sum_{i=1}^T \left(\widehat{\text{MMD}}(\hat{Q}_t \| Q_t) + \frac{\lambda_t}{N_1} \sum_{i=1}^{N_1} \|G_t(x_i^t) - x_i^t\|^2 \right). \quad (16)$$

The difference is as follows. Specifically, the t -th term $\widehat{\text{MMD}}(\hat{Q}_t \| Q_t) + \frac{\lambda_t}{N_1} \sum_{i=1}^{N_1} \|G_t(x_i^t) - x_i^t\|^2$, which we refer to as $\widehat{\text{MMD}}_t$, involves the first t transformation functions G_1, \dots, G_t . By viewing the forecast step as a special activation layer, training $G_{1:t}$ together under the loss $\widehat{\text{MMD}}_t$ is equivalent to training a deep neural network (NN), which can be seen as a stack of t small NNs (Figure 1). This joint optimization procedure, therefore, allows the transformations at different time steps to collaborate more effectively with each other for a better fit of the target posteriors. In contrast, in the sequential optimization approach, the transformations from earlier time steps are fixed once trained, preventing them from aiding subsequent transformations in improving their approximations. We refer to this joint optimization version of ATPF as ATPF-JO.

4 Theoretical Properties

4.1 Upper Bounds on the Excess Risk

In this section, we apply techniques from empirical process theory to derive bounds on the excess risk for our method. To ensure that the model remains well-posed and avoids singularities or divergence, we first introduce some common assumptions on the regularity of SSMs and the collection of test functions (Agapiou et al., 2017; Györfi et al., 2002; Lange, 2024).

Assumption 1 (Continuity and differentiability). *For each $t = 1, \dots, T$, $\mathcal{M}_t, \mathcal{H}_t \in C(\mathbb{R}^d)$ and $p_{\eta_t}, p_{\varepsilon_t} \in C^1(\mathbb{R}^d)$.*

Assumption 2 (Bounded weights and test functions). *$\sup_{1 \leq t \leq T} \|w_t\|_\infty \vee \|\mathcal{F}_D\|_\infty \leq B$, where $\{w_t\}_{t=1}^T$ are the weights of the SNIS particles and $\|\mathcal{F}_D\|_\infty := \sup_{f \in \mathcal{F}_D} \|f\|_\infty$.*

Assumption 3 (Bounded variance). *$\sup_{1 \leq t \leq T} \mathbb{E}\eta_t^2 \vee \mathbb{E}\varepsilon_t^2 < \infty$.*

To better understand the excess risk, we first decompose it into three parts.

Theorem 1 (Decomposition of the excess risk). *The excess risk of the analysis step (also called the statistical error, i.e., $\text{MMD}(\hat{Q}_t \| Q_t) - \widehat{\text{MMD}}(\hat{Q}_t \| Q_t)$), can be uniformly upper bounded by the following sum of three components:*

$$\begin{aligned} & \sup_{f \in \mathcal{F}_D} \left| \mathbb{E}_{y \sim Q_t} f(y) - \mathbb{E}_{x' \sim P_t} \left[\frac{\sum_{j=1}^{N_2} w_t(x'_j) f(x'_j)}{\sum_{j=1}^{N_2} w_t(x'_j)} \right] \right| + \sup_{f \in \mathcal{F}_D} \left| \mathbb{E}_{x' \sim P_t} \left[\frac{\sum_{j=1}^{N_2} w_t(x'_j) f(x'_j)}{\sum_{j=1}^{N_2} w_t(x'_j)} \right] - \frac{\sum_{j=1}^{N_2} w_t(x'_j) f(x'_j)}{\sum_{j=1}^{N_2} w_t(x'_j)} \right| \\ & + \sup_{h \in \mathcal{F}_D \circ \mathcal{G}_t} \left| \frac{1}{N_1} \sum_{i=1}^{N_1} h(x_i) - \mathbb{E}_{x \sim \hat{P}_t} h(x) \right| \end{aligned} \quad (17)$$

for all $\hat{Q}_t = G_{t\#} \hat{P}_t$ where $G_t \in \mathcal{G}_t$.

The first term represents the bias of the SNIS, which has a convergence rate of $O(\frac{1}{N_2})$ (Theorem 2.1 in Agapiou et al. (2017), Theorem 3 in Appendix A). The second term reflects the randomness inherent in the stochastically weighted empirical process of the SNIS estimator. Ensuring a sharp convergence rate for this term requires additional techniques and concentration conditions (see Lemma 1 in Appendix A). Specifically, the following assumptions are commonly used in related work (e.g., Liang, 2021; Oko et al., 2023; Magazinov & Peled, 2022; Saumard & Wellner, 2014).

Assumption 4 (Smoothness). Both $f(x)$ and $w_t(x)$ are differentiable for all $f \in \mathcal{F}_D$ and $t = 1, \dots, T$. Moreover, they are β -Lipschitz, i.e., $\|\nabla f(x)\|_2 \vee \|\nabla w_t(x)\| \leq \beta$.

Assumption 5 (Concavity). For all $t = 1, \dots, T$, the distribution P_t is strongly log-concave with parameter $\gamma_t > 0$.

Note that Assumptions 4 and 5 are not necessary for the convergence of our method. However, they play a crucial role to ensure a faster exponential rate of $O(\exp(-N_2))$. Without these assumptions, the rate reduces to $O(\frac{1}{N_2})$. For further details, please refer to Theorems 4 and 6 in Appendix A. With these assumptions and the decomposition of the excess risk, we derive the following nonasymptotic upper bound for our proposed method.

Theorem 2 (Upper bound on the excess risk). Assume Assumptions 1–5 hold. Let $\mathcal{N}_k(\varepsilon, \cdot)$ denote the L_k ε -covering number and $\mathcal{N}_k(\varepsilon, \cdot, X^{1:n})$ denote the empirical L_k ε -covering number with the empirical L_k metric. Then

$$\begin{aligned} & \mathbb{P} \left(\sup_{G_t \in \mathcal{G}_t} \left| \text{MMD}(G_{t\#} \hat{P}_t \| Q_t) - \widehat{\text{MMD}}(G_{t\#} \hat{P}_t \| Q_t) \right| > \varepsilon + \frac{12B(\chi^2(Q_t \| P_t) + 1)}{N_2} \right) \\ & \leq 2\mathcal{N}_\infty \left(\frac{\varepsilon}{6}, \mathcal{F}_D \right) \exp \left(-\frac{\gamma_t N_2 (\mathbb{E} w_t)^2 \varepsilon^2}{5760 B^2 \beta^2} \right) + 2 \exp \left(-\frac{N_2 (\mathbb{E} w_t)^2}{2B^2} \right) \\ & \quad + 8\mathcal{N}_\infty \left(\frac{\varepsilon}{32}, \mathcal{F}_D \right) \mathbb{E}_{X \sim \hat{P}_t} \mathcal{N}_1 \left(\frac{\varepsilon}{32\beta}, \mathcal{G}_t, X^{1:N_1} \right) \exp \left(-\frac{N_1 \varepsilon^2}{2048 B^2} \right), \end{aligned} \quad (18)$$

where $\chi^2(Q_t \| P_t) = \int (\frac{dQ_t}{dP_t} - 1)^2 dP_t$ is the χ^2 divergence between Q_t and P_t . As a consequence, for any $\delta > 0$, there exist $N_1(\delta)$ and $N_2(\delta)$, such that when $N_1 \geq N_1(\delta)$, $N_2 \geq N_2(\delta)$, with probability at least $1 - \delta$, the following inequality holds simultaneously and uniformly for all $\hat{Q}_t = G_{t\#} \hat{P}_t$ over $G_t \in \mathcal{G}_t$:

$$\begin{aligned} \text{MMD}(\hat{G}_{t\#} \hat{P}_t \| Q_t) & \leq \inf_{G_t \in \mathcal{G}_t} \text{MMD}(G_{t\#} \hat{P}_t \| Q_t) + \frac{24B(\chi^2(Q_t \| P_t) + 1)}{N_2} \\ & \quad + \left(\frac{128B\beta}{\sqrt{\gamma_t}(\mathbb{E} w_t)} \sqrt{\frac{\log \mathcal{N}_\infty(\frac{\varepsilon(\delta)}{6}, \mathcal{F}_D)}{N_2}} + 128B \sqrt{\frac{\log \mathcal{N}_\infty(\frac{\varepsilon(\delta)}{32}, \mathcal{F}_D) + \log \mathbb{E} \mathcal{N}_1(\frac{\varepsilon(\delta)}{32\beta}, \mathcal{G}_t)}{N_1}} \right) \sqrt{\log \frac{3}{\delta}}. \end{aligned} \quad (19)$$

The term $\text{MMD}(\hat{G}_{t\#} \hat{P}_t \| Q_t)$ represents the loss of our empirical estimate defined in equation 9 and the term $\inf_{G_t \in \mathcal{G}_t} \text{MMD}(G_{t\#} \hat{P}_t \| Q_t)$ represents the approximation error. In fact, $\text{MMD}(\hat{G}_{t\#} \hat{P}_t \| Q_t) - \inf_{G_t \in \mathcal{G}_t} \text{MMD}(G_{t\#} \hat{P}_t \| Q_t)$ is the statistical error. The other three terms appearing on the right-hand side of equation 19 correspond to the three terms in the decomposition equation 17. For the first term, the χ^2 divergence reflects the level of weight decay and a larger value means a severer decay and thus a slower convergence rate. For the second term, the factor $\frac{\beta}{\sqrt{\gamma_t}}$ means that stronger log-concavity and Lipschitzity help to accelerate the convergence. This is reasonable since (1) a stronger log-concavity in P_t implies that this distribution is relatively easier to estimate by finite samples, and (2) a stronger Lipschitzity in w_t implies that the importance sampling in the analysis step is more effective. The factor $\mathbb{E} w_t$ also acts as an indicator of the weight decay. For the third term, it is a standard rate with a parameter β . The law of convergence is the same as before: the larger value β takes, the slower rate the model will converge at.

Concretely, we can consider the case that Q_t and \mathcal{F}_D both refer to the Sobolev space $W^{\alpha,2}(1)$. Let N_1 go to infinity and take expectations on $X^{1:N_2}$. Then the term $\mathcal{N}_\infty(\mathcal{F}_D)$ can be replaced by its Dudley entropy integral, and the convergence rate would recover the vanilla GANs' rate $N_2^{-\frac{\alpha}{d}} \vee \frac{\log N_2}{\sqrt{N_2}}$ (Lemma 26 and Theorem 9 in Liang (2021)). This is because the bias of the SNIS estimator goes to zero as

N_2 goes to infinity. In our experiments, we always set a relatively large N_2 , say 10000, to mitigate the negative effects caused by the SNIS bias and weight decay.

Up to now, we have shown the bound on the excess risk in the analysis step. Next, we generalize our result to the forecast step.

Proposition 2 (An upper bound on the forecast error). *Assume Assumptions 1–4 hold. If \mathcal{M}_t is γ -Lipschitz, then*

$$\text{MMD}(\hat{P}_{t+1} \| P_{t+1}) = \text{MMD}(\mathcal{M}_{t\#} \hat{Q}_t * p_{\eta_{t+1}} \| \mathcal{M}_{t\#} Q_t * p_{\eta_{t+1}}) \leq \beta \gamma W_2(\hat{Q}_t \| Q_t), \quad (20)$$

where “ $*$ ” denotes the convolution operator.

A straightforward condition to ensure that \mathcal{M}_t is γ -Lipschitz is to set $\mathcal{M}_t \equiv \text{id}$, as considered in Lange (2024). Here, we extend this condition to a more general case under the Lipschitz continuity assumption. Notably, the MMD metric may be weaker than the W_2 metric, especially when the test function space is relatively small. Therefore, with assumptions 1-5, we cannot ensure the convergence of $W_2(\hat{Q}_t \| Q_t)$. Nevertheless, we establish an alternative bound for our kernel ATPF, which is detailed below.

Proposition 3 (An alternative upper bound on the forecast error). *Assume Assumptions 1–4 hold and we adopt the unit ball of the RKHS for \mathcal{F}_D as described in Section 3.1. If the contraction condition holds, i.e., $\|\mathcal{F}_D \circ \mathcal{M}_t\|_{\mathcal{H}} \leq \Omega \|\mathcal{F}_D\|_{\mathcal{H}}$ with an absolute constant Ω , then*

$$\text{MMD}(\mathcal{M}_{t\#} \hat{Q}_t * p_{\eta_{t+1}} \| \mathcal{M}_{t\#} Q_t * p_{\eta_{t+1}}) \leq \Omega \cdot \text{MMD}(\hat{Q}_t \| Q_t) + 2\beta \cdot \text{trace}(\text{Var}(\eta_{t+1}))^{\frac{1}{2}}. \quad (21)$$

The additional term $\text{trace}(\text{Var}(\eta_{t+1}))^{\frac{1}{2}}$ is due to the evolution noise, which cannot be neglected. Similar results can also be found in Proposition 2 of Lange (2024).

4.2 Convergence Rate Analysis

In this section, we derive upper bounds for the covering numbers involved in Theorem 2, which allows us to establish convergence rates of our method. When \mathcal{F}_D denotes an RKHS, Lemma D.2 in Yang et al. (2020) provides two absolute constants C_3 and C_4 such that

$$\log \mathcal{N}_{\infty}(\varepsilon, \mathcal{F}_D) \leq \begin{cases} C_3 \gamma [\log(B/\varepsilon) + C_4] & (\gamma\text{-finite spectrum}) \\ C_3 [\log(B/\varepsilon) + C_4]^{1+1/\gamma} & (\gamma\text{-exponential decay}) \\ C_3 (B/\varepsilon)^{2/[\gamma(1-2\tau)-1]} [\log(B/\varepsilon) + C_4] & (\gamma\text{-polynomial decay}) \end{cases} \quad (22)$$

where these three cases correspond to different eigenvalue decay rates. In this paper, we mainly focus on the linear kernel $K(x, y) = x^T y + c$, which corresponds to the first case with $\gamma = d$, and the Gaussian kernel $K(x, y) = \exp\left(-\frac{\|x - y\|_2^2}{2w^2}\right)$, which corresponds to the second case with $\gamma = \frac{1}{d}$.

We now focus on $\log \mathcal{N}_{\infty}(\varepsilon, \mathcal{G}_t)$. Specifically, here we adopt the neural network parameterization method in Suzuki (2019), where $\mathcal{G}_t = \Phi(L, W, S, R) := \{(A^{(L)} \text{ReLU}(\cdot) + b^{(L)}) \circ \dots \circ (A^{(1)} x + b^{(1)}) | A^{(i)} \in \mathbb{R}^{W_i \times W_{i+1}}, b^{(i)} \in \mathbb{R}^{W_{i+1}}, \sum_{i=1}^L (\|A^{(i)}\|_0 + \|b^{(i)}\|_0) \leq S, \max_i \|A^{(i)}\|_{\infty} \vee \|b^{(i)}\|_{\infty} \leq R\}$. Note that results for this fully-connected neural networks can be easily translated into other architectures (e.g., Petersen & Voigtlaender (2018); Ramesh et al. (2022)). By Lemma 3 in Suzuki (2019), there exists an absolute

constant C_5 such that

$$\log \mathcal{N}_\infty(\varepsilon, \mathcal{G}_t, \|\cdot\|_{L_\infty[-M, M]^d}) \leq 2C_5 SL \log(\varepsilon^{-1} L \|W\|_\infty (R \vee 1) M). \quad (23)$$

Note that this bound is only valid for distributions with compact support. It is necessary to extend this result to sub-Gaussian cases since the noises involved in SSMs are usually not bounded but sub-Gaussian. We summarize it in the following corollary.

Corollary 1 (Bound on log-covering number in sub-Gaussian cases). *If we assume that for each t , all mentioned distributions are sub-Gaussian with uniform sub-Gaussian parameter σ_t , then there exists an absolute constant C_7 such that the following inequality holds with probability at least $1 - \exp\left(-\frac{N_1 \varepsilon^2}{2048 B^2}\right)$:*

$$\log \mathcal{N}_1\left(\frac{\varepsilon}{32\beta}, \mathcal{G}_t, X^{1:N_1}\right) \leq 2C_7 SL \log\left(\beta L \|W\|_\infty (R \vee 1) \sigma_t \sqrt{\frac{\log(2dN_1)}{\varepsilon^2} + \frac{N_1}{2048 B^2}}\right). \quad (24)$$

Note that the growth rate of the log-covering number is $O(\log(N_1))$. Thus, the convergence rate in sub-Gaussian cases will be slower by a factor $\log(N_1)$ than that in bounded cases.

After analyzing the covering number of these two spaces, we can now derive the convergence rate for our proposed kernel ATPF methods with some standard neural network approximation theorems (Suzuki, 2019; Chakraborty & Bartlett, 2024). Following these works, we consider the Besov space $B_{p,q}^s(\Omega)$ (see Definition 4 in Suzuki (2019)) and assume the following assumption.

Assumption 6. *There exists an oracle $G'_t \in B_{p,q}^s(\Omega)$ such that $G'_{t\#} \hat{P}_t = Q_t$.*

Since high-probability bounds can be directly derived by plugging these log-covering number bounds into equation 19, in the following we focus more on the entropy integral, which further leads to the bound on $\mathbb{E}\text{MMD}(\hat{G}_{t\#} \hat{P}_t \| Q_t)$. We observe that the Gaussian kernel may lack scalability in high-dimensional settings, as its approximation error is significantly affected by the curse of dimensionality. Specifically, we can establish the following convergence rate.

Proposition 4 (Convergence rate of the Gaussian kernel MMD). *Assume Assumptions 1–6 hold and that all mentioned distributions are sub-Gaussian. Let $s > \frac{d}{p}$. If we adopt the unit ball of the Gaussian RKHS for \mathcal{F}_D and parameterize \mathcal{G}_t by the NN set $\Phi(L, W, S, R)$, then the following convergence rate holds:*

$$\mathbb{E}\text{MMD}(\hat{G}_{t\#} \hat{P}_t \| Q_t) \lesssim (\log N_1)^{\frac{s}{2}} \vee N_1^{-\frac{s}{2(s+d)}} + N_2^{-\frac{1}{2}}. \quad (25)$$

Moreover, when the linear kernel is adopted, we have the following convergence rate for the posterior mean estimate.

Proposition 5 (Convergence rate of the posterior mean). *Assume Assumptions 1–5 hold and that all mentioned distributions are sub-Gaussian. If we adopt the unit ball of the linear RKHS for \mathcal{F}_D and parameterize \mathcal{G}_t by the NN set $\Phi(L, W, S, R)$, the convergence rate of the posterior mean is*

$$\|\mathbb{E}_{X \sim \hat{G}_{t\#} \hat{P}_t} X - \mathbb{E}_{Y \sim Q_t} Y\|_2 \lesssim d \left(\frac{\log N_1}{\sqrt{N_1}} + \frac{1}{\sqrt{N_2}} \right) \quad (26)$$

if $R \geq \|\mathbb{E}_{Y \sim Q_t} Y\|_\infty$. Here, $\mathbb{E}_{X \sim \hat{G}_{t\#} \hat{P}_t} X$ is the estimated posterior mean and $\mathbb{E}_{Y \sim Q_t} Y$ is the true posterior mean.

5 Experiments

In this section, we compare our proposed ATPF with several data assimilation algorithms: EnKF (Katzfuss et al., 2020), ETPF (Reich, 2013), NLEAF (Lei & Bickel, 2011), PF (Gordon et al., 1993), MPF (Nakano et al., 2007) and PFGR (Xiong et al., 2006). Following Lei & Bickel (2011), we use NLEAF1 and NLEAF2 for Lorenz63 system and NLEAF1 and NLEAF1q for Lorenz96 system, where “1” stands for matching the first moment, “2” stands for matching the second moment and “1q” stands for quadratic regression.

We use the following settings for different approaches in our experiments. For ATPF methods, we simply set a time-homogeneous regularization parameter $\lambda_t \equiv \lambda$ for each t . For KATPF with Gaussian kernels, we set the bandwidth parameter w to be the median of all L_2 distances between each pair of particles (Liu & Wang, 2016). For other existing methods, we just follow the standard settings used in previous works. For PF series, we take the resampling step after each reweighting step. In addition, we adopt the inflation trick (see Appendix C or Lei & Bickel (2011)) for all filtering algorithms appearing in this section. We use the likelihood of the data as a criterion to select the optimal inflation parameters. All data sets and code are available at <https://github.com/WQgcx/ATPF.git>.

5.1 Nonlinear Simulation

In this section, we test the approximation accuracy of different methods on a nonlinear model where the EnKF method would fail to provide exact posterior estimate. More specifically, we consider the following simple 1-dimension 2-stage state-space model:

$$p(x_0) \sim \mathcal{N}(0, 1), \quad p(x_1|x_0) \sim \mathcal{N}(x_0^2 + \log(x_0^2 + 1), 0.1^2), \quad p(y_t|x_t) \sim \mathcal{N}(x_t, 1) \text{ for } t = 0, 1. \quad (27)$$

Although the observation y_t conditioned on the latent state x_t follows a standard Gaussian distribution, the true posterior of x_1 is non-Gaussian due to the nonlinear evolution from x_0 to x_1 . Mathematically speaking, this is because $p(x_1|y_0, y_1) \propto p(x_1|y_0)p(y_1|x_1)$; while $p(y_1|x_1)$ is Gaussian, $p(x_1|y_0)$ is not. Now assume that we already have the observations $y_0 = y_1 = 0$, our goal is to sample from the posterior $p(x_1|y_0, y_1)$ whose ground truth value can be obtained via numerical quadratures.

The regularization parameter λ corresponding to the vanilla ATPF (i.e., use the alternative optimization algorithm), Gaussian KATPF and linear KATPF is set to be 0.001, 0.0 and 0.2, respectively. Experimental results are shown in Figure 2. We use 10000 particles to demonstrate the approximation accuracy of the fitted posteriors from different methods. The blue lines represent the density of the true posterior $p(x_1|y_0, y_1)$ and the orange histograms represent the estimated posterior densities from different methods.

From Figure 2, we see that the true posterior is not a symmetric Gaussian, but instead exhibits a right-skewed distribution. Therefore, the core challenge in training and filtering is to accurately capture the shape of density around the peak. We see that the EnKF (top left panel) is limited to a Gaussian approximation which fails to capture the skewness. The NLEAF methods (top middle and top right panels) perform better, as they can capture the peak shape by matching either the first or second moments. The vanilla PF (middle left panel) is the best estimator in this case, as it is asymptotically unbiased and well suits this low-dimensional scenario. MPF (center panel) enhances particle diversity and stability, though it does so at the price of some statistical consistency by allowing more outliers. ETPF (middle right panel), which relies on a linear programming algorithm, tends to produce some indented protuberances, possibly due to the lack of randomness in its design. As for our proposed methods, they

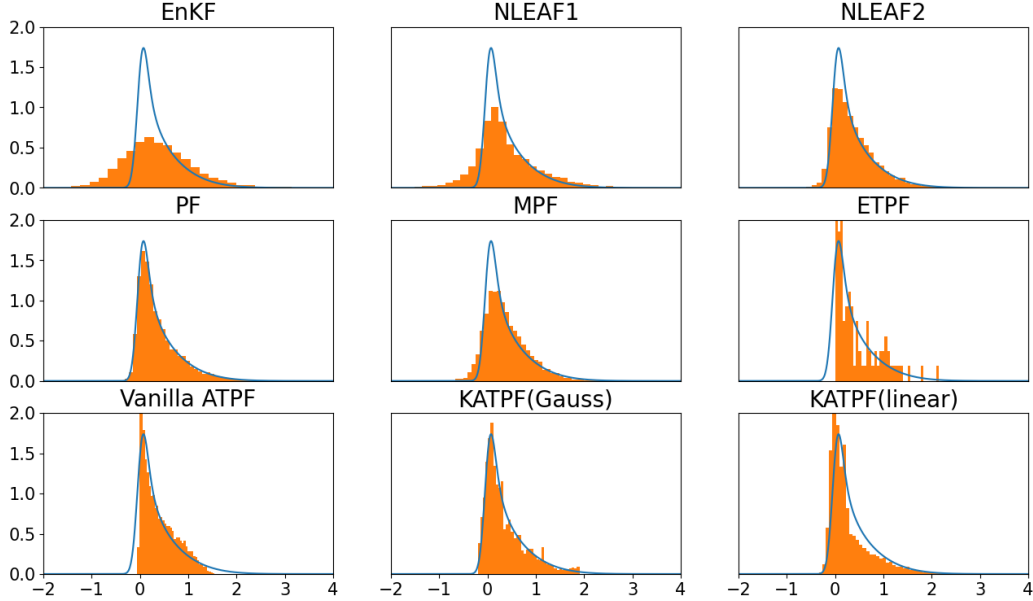


Figure 2: Experimental results of a simple two-stage state-space model.

all capture the general shape of the target distribution well. More specifically, the vanilla ATPF (bottom left panel) provide particles that concentrate on the mode, and the linear KATPF (bottom right) tends to underestimate the skewness of the density and would benefit from additional W_2 regularization to correct this. In this low-dimensional case, the Gaussian kernel performs particularly well. The corresponding RKHS manages to provide a rich set of test functions, leading to the best performance among all ATPF variants (bottom middle panel).

5.2 Filtering the Rainfall Data

In this section, we consider the threshold observation model for rainfall (e.g., [Sanso & Guenni \(1999\)](#)). The observations are modeled as $y_{t,l} = z_{t,l}^{\theta_t} \mathbf{1}_{z_{t,l} > 0}$ for $l = 1, \dots, d$ and some $\theta_t > 1$, and $z_t | x_t \sim \mathcal{N}(H_t x_t, \sigma_t^2)$. Here, z_t is an unknown auxiliary variable which connects the latent state x_t and the actual observation y_t . This kind of two-stage observation rule defines a rain-fall type distribution, i.e., a mixture of a positive right-skewed distribution, with a point mass at zero (e.g., [Sanso & Guenni \(1999\)](#); [Katzfuss et al. \(2020\)](#)). The parameter θ_t , which controls the skewness, is either known or assigned with a pre-specified prior. The whole rainfall model can be mathematically depicted as

$$\begin{aligned} x_t | x_{t-1} &\sim \mathcal{N}(\mathcal{M}_{t-1}(x_{t-1}), Q_t), & z_t | x_t &\sim \mathcal{N}(H_t x_t, \sigma_t^2), & \theta_t &\sim p(\theta_t), \\ y_{t,l} | z_{t,l}, \theta_t &= z_{t,l}^{\theta_t} \mathbf{1}_{z_{t,l} > 0}, & \text{for } l = 1, \dots, d. \end{aligned} \quad (28)$$

Following [Katzfuss et al. \(2020\)](#), we focus on the analysis step, that is, how to transport the prior particles to the posterior ones. We first simulate 100 true state vectors on a one-dimensional spatial domain $[1, 100]$ according to a Gaussian Process (GP) prior with the following exponential kernel:

$$(x_1, \dots, x_d) \sim \mathcal{N}_d(\mu, \Sigma) \text{ with } \Sigma_{ij} = \alpha_1 \exp\left(-\frac{|i-j|}{\alpha_2}\right), \quad (29)$$

where α_1 is the scale parameter and α_2 is the width parameter. In our experiments, we set $d = 100$, $\mu = (0, \dots, 0)^T$, $\alpha_1 = 1$ and $\alpha_2 = 20$. As for the rainfall model itself, we set $H_t \equiv I_{100 \times 100}$ and $\sigma_t \equiv 0.4$. And for simplicity, we set $\theta_t \equiv 3$, i.e., $p(\theta_t) = \delta(\theta_t - 3)$.

Table 1: Experimental results (RMSE) of the rainfall model.

MCMC	EnKF	NLEAF1	NLEAF2	PF	KATPF(Gauss)	KATPF(linear)
0.1245	0.2422	0.1717	0.1752	0.1433	0.1209	0.1394

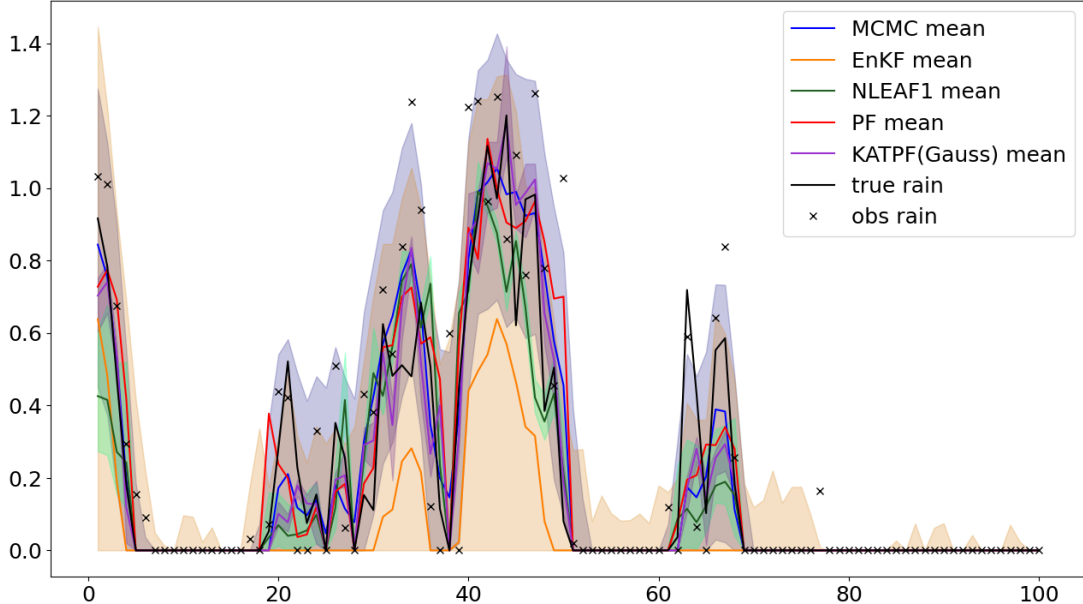


Figure 3: Experimental results of the rainfall model. The shaded areas represent the corresponding 95% confidence intervals (CIs).

As in [Katzfuss et al. \(2020\)](#), we truncate all particles in the posterior estimates at 0 as negative rainfall values are not physically meaningful. We compute RMSEs over the true rain and treat the estimate obtained by the first-order Langevin method ([Welling & Teh, 2011](#)) (running 10000 steps for 500 independent chains and collecting the final samples) as the exact posterior. Experimental results are presented in [Figure 3](#), with corresponding RMSE values shown in [Table 1](#). We use 100000 particles for the PF and 500 particles for the other filtering methods. The 95% credit intervals are constructed based on the ensemble.

From [Table 1](#), we see that our ATPF methods outperform their teacher (i.e., PF) with much fewer particles. This is partly due to the explicit regularization of W_2 distance and implicit regularization of neural network parameterization and the corresponding stochastic optimization algorithms ([Ma et al., 2018](#); [Wei et al., 2020](#)). While the PF relies solely on a mixture of delta functions to approximate the density, our KATPF method introduces smoother approximations, akin to other kernel-based methods, which results in improved performance. This trend is consistent across the subsequent experiments.

From [Figure 3](#), we observe that the EnKF tends to significantly underestimate the true rainfall while NLEAF-type methods are less robust to outliers, as evidenced by their narrower confidence intervals (CIs) that sometimes fail to cover the true data. In fact, except for the EnKF, nearly all baseline filtering methods produce narrower and bumpier CIs than the exact posterior during the peak period, indicating that prediction with this rainfall model is challenging due to the strong randomness assumption and truncated observations. On the other hand, our proposed methods strike a good balance between the accuracy of point estimates and the uncertainty in the posterior approximations, thanks to the adversarial framework. This results in more accurate estimates than the EnKF (see [Table 1](#)) and more reasonable CIs than NLEAF methods (see [Figure 3](#)). Notably, the Gaussian KATPF outperforms all the other

Table 2: Experimental results (RMSE) of the Lorenz63 system.

	EnKF	NLEAF1	NLEAF2	PF	MPF	PFGR	KATPF (Gauss)	KATPF (linear)	KATPF-JO (linear)
$T = 100$ $\Delta t = 0.02$	0.1924	0.1862	0.1907	0.1719	0.2295	0.2110	0.1946	0.1891	0.1398
$T = 2000$ $\Delta t = 0.02$	0.1142	0.1133	0.1063	0.1131	0.1287	0.1476	0.1111	0.1087	0.0843
$T = 2000$ $\Delta t = 0.04$	0.1870	0.1716	0.1475	0.1465	0.1970	0.1874	0.1608	0.1544	0.1157
$T = 2000$ $\Delta t = 0.06$	0.1824	0.1769	0.1445	0.1503	0.1968	0.1759	0.1769	0.1506	0.0973
$T = 2000$ $\Delta t = 0.08$	0.2293	0.2140	0.1751	0.1825	0.2343	0.2081	0.1858	0.1829	0.1305

filtering algorithms in terms of RMSE, even though it was not trained by minimizing the square loss.

5.3 The Lorenz63 Model

As a chaotic system, the Lorenz63 model is described by the following set of ordinary differential equations:

$$\begin{aligned}
 \frac{dx_\tau(1)}{d\tau} &= -\sigma x_\tau(1) + \sigma x_\tau(2), \\
 \frac{dx_\tau(2)}{d\tau} &= -x_\tau(1)x_\tau(3) + \rho x_\tau(1) - x_\tau(2), \\
 \frac{dx_\tau(3)}{d\tau} &= x_\tau(1)x_\tau(2) - \beta x_\tau(3),
 \end{aligned}
 \tag{30}$$

where τ is the continuous time index, x_τ is a three-dimensional latent state variable representing a simplified model of a heated fluid’s flow, with parameters $\beta = \frac{8}{3}$, $\rho = 28$, and $\sigma = 10$. Note that this model does not include evolution noise, which implies $\mathbb{P}(\eta_t = 0) = 1$ in equation 2.

In the simulation, we use standard Euler discretization with a small time step $\delta t = 0.02$ to numerically integrate this continuous-time Lorenz63 model. The observation rule is set as $y_t|x_t \sim \mathcal{N}(x_t, I_{3 \times 3})$ and data are generated by observing $T = 100$ or $T = 2000$ samples from the system. The goal is to evaluate the performance of different methods in both short-term and long-term evolution scenarios. In addition, the time interval between consecutive observations is set to be $\Delta t = 0.02, 0.04, 0.06$ or 0.08 , corresponding to 1, 2, 3 or 4 Euler discretization steps between x_{t-1} and x_t (or y_{t-1} and y_t), respectively. Here, larger observation gaps typically introduce more nonlinearities in the evolution. We use 1000 particles in all experiments.

Table 2 shows the RMSE between the true values and the ensemble mean (Lei & Bickel, 2011). We see that our KATPF methods consistently outperform the other baselines, particularly when the nonlinearity increases. Specifically, when the observation interval Δt is small (i.e., the first two rows), the evolution model is nearly linear due to the Euler discretization, and all methods perform similarly. As Δt increases, the filtering task becomes more challenging due to the increasing nonlinearity of the evolution model, leading to a general decline in performance across all methods. However, KATPF methods exhibit a slower rate of performance degradation compared to the others. From Figure 8, we can see that as non-linearity increases, the particle trajectories become more chaotic, making it harder to accurately identify them. Despite this, our method maintains strong performance. The results also reveal that the joint optimization procedure (ATPF-JO) outperforms the sequential training approach. See more results on the effect of the OT regularization in Appendix B (Table 4).

Table 3: Experimental results (RMSE) of the Lorenz96 model.

	EnKF (w/tap.)	NLEAF1 (w/loc.)	NLEAF1q (w/loc.)	PF	MPF	KATPF (Gauss)	KATPF (linear)	KATPF-JO (linear)
$T = 100$ $\Delta t = 0.01$	0.4212	0.3895	0.4620	0.5478	0.4457	0.4250	0.4133	0.3927
$T = 1000$ $\Delta t = 0.01$	0.2125	0.2133	0.2374	0.2733	0.2170	0.2155	0.1920	0.1600
$T = 10$ $\Delta t = 0.2$	0.8320	0.8036	0.9043	0.8498	0.8079	0.8649	0.7860	0.7723

5.4 The Lorenz96 Model

The Lorenz96 model is another commonly used testbed for evaluating data assimilation methods. The 40-dimensional state vector evolves according to the following system of ordinary differential equations:

$$\frac{dx_\tau(i)}{d\tau} = [x_\tau(i+1) - x_\tau(i-2)]x_\tau(i-1) - x_\tau(i) + 8 \text{ for } i = 1, \dots, 40, \quad (31)$$

where periodic boundary conditions are applied: $x_\tau(0) = x_\tau(40)$, $x_\tau(-1) = x_\tau(39)$ and $x_\tau(41) = x_\tau(1)$. This model is widely used for studying chaotic behavior and turbulence in atmospheric and climate systems. Also, this model does not include evolution noise.

Due to the complexity of the Lorenz96 model, we set the discretization step size to $\delta = 0.01$ in the simulation. To increase the difficulty of fitting, we adopt the hard case setup from [Lei & Bickel \(2011\)](#) where the observation rule is given by $y_t = H_t x_t + \varepsilon_t$ equation 5 with $H_t = (e_1, e_3, \dots, e_{39})_{40 \times 20}$ and $\varepsilon_t \sim \mathcal{N}(0, I_{20 \times 20})$. Here, $e_i = (0, \dots, 0, \underbrace{1}_{i\text{-th}}, 0, \dots, 0)$ is the standard basis vector with all zero entries except the i th position. This means that only 20 out of the 40 coordinates of the state vector are observed at each time step, with each observation contaminated by standard Gaussian noise. We generate data by simulating $T = 100$ or $T = 1000$ samples from this model with $\Delta t = 0.01$ (i.e., only one discretization step between x_{t-1} and x_t). To further enhance nonlinearity, we also consider a case with $\delta = 0.02$, $\Delta t = 0.2$ and $T = 10$, similar to [Katzfuss et al. \(2020\)](#). To better handle the high-dimensional nature of the system, we use localization for the NLEAF methods (denoted as “w/ loc.”) and the tapering method for the EnKF (denoted as “w/tap.”). The extra hyperparameters involved are chosen according to [Lei & Bickel \(2011\)](#). For our proposed ATPF methods, we use MPF as a guidance mechanism, which helps alleviate weight degeneracy in this high-dimensional setting. All filtering algorithms adopt the inflation trick introduced in Appendix C. For the EnKF, NLEAF series, and our proposed KATPF, we used 500 particles, which we found to be sufficient in our experiments. For PF series, we use 30000 particles (and 10^6 particles for the third case) to ensure numerical stability and statistical consistency.

Table 3 shows the RMSEs of different methods across three different scenarios. We see that KATPF methods perform well in all three cases, even outperforming their teacher method (i.e., MPF) with significantly fewer particles. Although NLEAF1 performs well in short-term settings (when T is small), KATPF methods exhibit stronger capacities, especially in long-term settings. Again, with joint optimization, the KATPF-JO performs the best among all KATPF variants.

6 Conclusion and Discussion

In this paper, we propose the adversarial transform particle filter (ATPF), a new filtering method for data assimilation in nonlinear and non-Gaussian models. ATPF combines the particle diversity of EnKFs with

the statistical consistency of PFs within an adversarial framework that minimizes the maximum mean discrepancy (MMD) to match the posterior distribution. We provide theoretical guarantees for ATPF’s consistency and convergence, and validate its accuracy and effectiveness through extensive experiments. Additionally, optimal transport based regularization can be employed to enhance performance. We also show that existing techniques, such as the inflation trick, can be seamlessly incorporated into our method.

Despite its advantages, fitting high dimensional models directly with ATPF remains challenging as it relies on particle filters (or their variants) to estimate posterior expectations, and the importance sampling required for this becomes difficult in high-dimensional settings (see the property of the χ^2 divergence in Theorem 3). However, unlike PFs that use importance sampling to estimate the whole posterior distribution, ATPF only uses importance sampling to estimate the posterior expectation of test functions. This is similar to NLEAF (Lei & Bickel, 2011), which lends itself more easily to localization for dimension reduction. Another remedy would be to introduce a sequence of auxiliary distributions that interpolate between the prior and the posterior (e.g., the annealing path (Geyer, 1991)). By learning transformations to map between successive distributions using ATPF, we could more easily achieve better approximations, as successive distributions can be made closer to each other. We leave the investigation of more efficient ATPF methods for high-dimensional models to future work.

Acknowledgments

This research was supported by National Natural Science Foundation of China grants 12292980. The research of Cheng Zhang was supported in part by National Natural Science Foundation of China (grant no. 12201014 and grant no. 12292983), the National Engineering Laboratory for Big Data Analysis and Applications, the Key Laboratory of Mathematics and Its Applications (LMAM), and the Fundamental Research Funds for the Central Universities, Peking University. The research of Wei Lin was supported in part by National Natural Science Foundation of China (grant no. 12171012 and grant no. 12292981).

References

- Sergios Agapiou, Omiros Papaspiliopoulos, Daniel Sanz-Alonso, and Andrew M Stuart. Importance sampling: Intrinsic dimension and computational cost. *Statistical Science*, pp. 405–431, 2017. [8](#), [22](#), [25](#)
- Michael G Akritas. Empirical processes associated with v-statistics and a class of estimators under random censoring. *The Annals of Statistics*, pp. 619–637, 1986. [6](#)
- Mauricio A Alvarez, Lorenzo Rosasco, Neil D Lawrence, et al. Kernels for vector-valued functions: A review. *Foundations and Trends® in Machine Learning*, 4(3):195–266, 2012. [22](#)
- Jeffrey L Anderson. An ensemble adjustment kalman filter for data assimilation. *Monthly weather review*, 129(12):2884–2903, 2001. [1](#), [2](#)
- Jeffrey L Anderson. An adaptive covariance inflation error correction algorithm for ensemble filters. *Tellus A: Dynamic meteorology and oceanography*, 59(2):210–224, 2007. [2](#)
- Jeffrey L Anderson. A non-gaussian ensemble filter update for data assimilation. *Monthly Weather Review*, 138:4186–4198, 2010. [5](#)
- Martin Arjovsky, Soumith Chintala, and Léon Bottou. Wasserstein generative adversarial networks. In *International conference on machine learning*, pp. 214–223. PMLR, 2017. [2](#)
- M Sanjeev Arulampalam, Simon Maskell, Neil Gordon, and Tim Clapp. A tutorial on particle filters for online nonlinear/non-gaussian bayesian tracking. *IEEE Transactions on signal processing*, 50(2):174–188, 2002. [2](#), [4](#)
- Laurent Bertino, Geir Evensen, and Hans Wackernagel. Sequential data assimilation techniques in oceanography. *International Statistical Review*, 71(2):223–241, 2003. [1](#)
- Craig H Bishop, Brian J Etherton, and Sharanya J Majumdar. Adaptive sampling with the ensemble transform kalman filter. part i: Theoretical aspects. *Monthly weather review*, 129(3):420–436, 2001. [2](#)
- B. P. Carlin, N. G. Polson, and D. S. Stoffer. A monte carlo approach to nonnormal and nonlinear state-space modeling. *Journal of the American Statistical Association*, 87:493–500, 1992. [2](#)
- Saptarshi Chakraborty and Peter L Bartlett. On the statistical properties of generative adversarial models for low intrinsic data dimension. *arXiv preprint arXiv:2401.15801*, 2024. [11](#)
- Geir Evensen. Sequential data assimilation with a nonlinear quasi-geostrophic model using monte carlo methods to forecast error statistics. *Journal of Geophysical Research: Oceans*, 99(C5):10143–10162, 1994. [1](#), [2](#), [4](#)
- Geir Evensen. The ensemble kalman filter: Theoretical formulation and practical implementation. *Ocean dynamics*, 53:343–367, 2003. [2](#)
- Jiaojiao Fan, Qinsheng Zhang, Amirhossein Taghvaei, and Yongxin Chen. Variational wasserstein gradient flow. *arXiv preprint arXiv:2112.02424*, 2021. [7](#)
- Steven J Fletcher. *Data assimilation for the geosciences: From theory to application*. Elsevier, 2022. [1](#)
- Reinhard Furrer, Marc G Genton, and Douglas Nychka. Covariance tapering for interpolation of large spatial datasets. *Journal of Computational and Graphical Statistics*, 15(3):502–523, 2006. [2](#), [38](#)

- D. Gamerman. Markov chain monte carlo for dynamics generalized linear models. *Biometrika*, 85: 215–227, 1998. 2
- C. J. Geyer. Markov chain Monte Carlo maximum likelihood. *Interface Proceedings*, 1991. 17
- Ian Goodfellow, Jean Pouget-Abadie, Mehdi Mirza, Bing Xu, David Warde-Farley, Sherjil Ozair, Aaron Courville, and Yoshua Bengio. Generative adversarial nets. *Advances in neural information processing systems*, 27, 2014. 2
- Neil J Gordon, David J Salmond, and Adrian FM Smith. Novel approach to nonlinear/non-gaussian bayesian state estimation. In *IEE proceedings F (radar and signal processing)*, volume 140, pp. 107–113. IET, 1993. 1, 2, 3, 12
- László Györfi, Michael Kohler, Adam Krzyżak, and Harro Walk. *A Distribution-Free Theory of Non-parametric Regression*. 2002. URL <https://api.semanticscholar.org/CorpusID:43315484>. 8, 25
- Timothy Classen Hesterberg. *Advances in importance sampling*. Stanford University, 1988. 5
- Brian R Hunt, Eric J Kostelich, and Istvan Szunyogh. Efficient data assimilation for spatiotemporal chaos: A local ensemble transform kalman filter. *Physica D: Nonlinear Phenomena*, 230(1-2):112–126, 2007. 2, 38
- Richard Jordan, David Kinderlehrer, and Felix Otto. The variational formulation of the fokker–planck equation. *SIAM journal on mathematical analysis*, 29(1):1–17, 1998. 7
- R. E. Kalman. A new approach to linear filtering and prediction problems. *Journal of Basic Engineering*, 82:35–45, 1960. 2, 4
- Matthias Katzfuss, Jonathan R Stroud, and Christopher K Wikle. Understanding the ensemble kalman filter. *The American Statistician*, 70(4):350–357, 2016. 38
- Matthias Katzfuss, Jonathan R Stroud, and Christopher K Wikle. Ensemble kalman methods for high-dimensional hierarchical dynamic space-time models. *Journal of the American Statistical Association*, 115(530):866–885, 2020. 5, 12, 13, 14, 16
- Youngjoo Kim, Hyochoong Bang, et al. Introduction to kalman filter and its applications. *Introduction and Implementations of the Kalman Filter*, 1:1–16, 2018. 4
- Augustine Kong. A note on importance sampling using standardized weights. *University of Chicago, Dept. of Statistics, Tech. Rep*, 348:14, 1992. 3
- Hans R Künsch. Recursive monte carlo filters: algorithms and theoretical analysis. *Annals of Statistics*, pp. 1983–2021, 2005. 4
- Rutger-Jan Lange. Bellman filtering and smoothing for state–space models. *Journal of Econometrics*, 238(2):105632, 2024. 8, 10
- Jing Lei and Peter Bickel. A moment matching ensemble filter for nonlinear non-gaussian data assimilation. *Monthly Weather Review*, 139(12):3964–3973, 2011. 1, 2, 5, 12, 15, 16, 17, 38
- Tengyuan Liang. How well generative adversarial networks learn distributions. *Journal of Machine Learning Research*, 22(228):1–41, 2021. 8, 9, 30

- Qiang Liu and Dilin Wang. Stein variational gradient descent: A general purpose bayesian inference algorithm. *Advances in neural information processing systems*, 29, 2016. [12](#)
- Cong Ma, Kaizheng Wang, Yuejie Chi, and Yuxin Chen. Implicit regularization in nonconvex statistical estimation: Gradient descent converges linearly for phase retrieval and matrix completion. In *International Conference on Machine Learning*, pp. 3345–3354. PMLR, 2018. [14](#)
- Alexander Magazinov and Ron Peled. Concentration inequalities for log-concave distributions with applications to random surface fluctuations. *The Annals of Probability*, 50(2):735–770, 2022. [8](#)
- Michael Montemerlo, Sebastian Thrun, Daphne Koller, Ben Wegbreit, et al. Fastslam 2.0: An improved particle filtering algorithm for simultaneous localization and mapping that provably converges. In *IJCAI*, volume 3, pp. 1151–1156, 2003. [2](#)
- Kevin Murphy and Stuart Russell. Rao-blackwellised particle filtering for dynamic bayesian networks. In *Sequential Monte Carlo methods in practice*, pp. 499–515. Springer, 2001. [2](#)
- Christian Musso, Nadia Oudjane, and Francois Le Gland. Improving regularised particle filters. In *Sequential Monte Carlo methods in practice*, pp. 247–271. Springer, 2001. [4](#)
- Shinya Nakano, Genta Ueno, and Tomoyuki Higuchi. Merging particle filter for sequential data assimilation. *Nonlinear Processes in Geophysics*, 14(4):395–408, 2007. [2](#), [12](#)
- Kazusato Oko, Shunta Akiyama, and Taiji Suzuki. Diffusion models are minimax optimal distribution estimators. In *International Conference on Machine Learning*, pp. 26517–26582. PMLR, 2023. [8](#)
- Philipp Petersen and Felix Voigtlaender. Optimal approximation of piecewise smooth functions using deep relu neural networks. *Neural Networks*, 108:296–330, 2018. [10](#)
- Jonathan Poterjoy. A localized particle filter for high-dimensional nonlinear systems. *Monthly Weather Review*, 144(1):59–76, 2016. [7](#)
- Florence Rabier. Overview of global data assimilation developments in numerical weather-prediction centres. *Quarterly Journal of the Royal Meteorological Society: A journal of the atmospheric sciences, applied meteorology and physical oceanography*, 131(613):3215–3233, 2005. [1](#)
- Aditya Ramesh, Prafulla Dhariwal, Alex Nichol, Casey Chu, and Mark Chen. Hierarchical text-conditional image generation with clip latents. *arXiv preprint arXiv:2204.06125*, 1(2):3, 2022. [10](#)
- Sebastian Reich. A nonparametric ensemble transform method for bayesian inference. *SIAM Journal on Scientific Computing*, 35(4):A2013–A2024, 2013. [6](#), [7](#), [12](#)
- Bruno Sanso and Lelys Guenni. Venezuelan rainfall data analysed by using a bayesian space–time model. *Journal of the Royal Statistical Society: Series C (Applied Statistics)*, 48(3):345–362, 1999. [13](#)
- Adrien Saumard and Jon A Wellner. Log-concavity and strong log-concavity: a review. *Statistics surveys*, 8:45, 2014. [8](#)
- Robert J Serfling. *Approximation theorems of mathematical statistics*. John Wiley & Sons, 2009. [6](#)
- N. Shephard and M. Pitt. Likelihood analysis of non-gaussian measurement time series. *Biometrika*, 84: 653–667, 1997. [2](#)

- Alexander J Smola, A Gretton, and K Borgwardt. Maximum mean discrepancy. In *13th international conference, ICONIP*, pp. 3–6, 2006. [6](#)
- Chris Snyder, Thomas Bengtsson, Peter Bickel, and Jeff Anderson. Obstacles to high-dimensional particle filtering. *Monthly Weather Review*, 136(12):4629–4640, 2008. [2](#), [7](#)
- Hao-Xuan Sun, Shouxia Wang, Xiaogu Zheng, and Song Xi Chen. High-dimensional ensemble kalman filter with localization, inflation, and iterative updates. *Quarterly Journal of the Royal Meteorological Society*, 150(765):4870–4884, 2024. [2](#)
- Taiji Suzuki. Adaptivity of deep relu network for learning in besov and mixed smooth besov spaces: optimal rate and curse of dimensionality. In *International Conference on Learning Representations*, volume 7, 2019. [10](#), [11](#), [30](#)
- Martin Wainwright. *High-Dimensional Statistics: A Non-Asymptotic Viewpoint*. 2019. ISBN 9781108498029. doi: 10.1017/9781108627771. [23](#), [24](#)
- Colin Wei, Sham Kakade, and Tengyu Ma. The implicit and explicit regularization effects of dropout. In *International Conference on Machine Learning*, pp. 10181–10192. PMLR, 2020. [14](#)
- Max Welling and Yee W Teh. Bayesian learning via stochastic gradient langevin dynamics. In *Proceedings of the 28th international conference on machine learning (ICML-11)*, pp. 681–688. Citeseer, 2011. [14](#)
- Xiaozhen Xiong, Ionel Michael Navon, and Bahri Uzunoglu. A note on the particle filter with posterior gaussian resampling. *Tellus A: Dynamic Meteorology and Oceanography*, 58(4):456–460, 2006. [2](#), [12](#)
- Chen Xu, Xiuyuan Cheng, and Yao Xie. Normalizing flow neural networks by jko scheme. *Advances in Neural Information Processing Systems*, 36, 2024. [7](#)
- Zhuoran Yang, Chi Jin, Zhaoran Wang, Mengdi Wang, and Michael I Jordan. On function approximation in reinforcement learning: Optimism in the face of large state spaces. *arXiv preprint arXiv:2011.04622*, 2020. [10](#)

Supplementary Material for “Adversarial Transform Particle Filters”

A Proofs

Definition 1 (RKHS, Alvarez et al. (2012)). *A bivariate, symmetric and positive definite function $K(\cdot, \cdot)$ defined on the domain E is called a reproducing kernel for a Hilbert space \mathcal{H} if it satisfies the following two properties:*

(a) $\forall x \in E, K(\cdot, x) \in \mathcal{H}$;

(b) (Reproducing property) $\forall f \in \mathcal{H}$ and $x \in E, f(x) = \langle f, K(\cdot, x) \rangle_{\mathcal{H}}$.

When such a reproducing kernel exists, \mathcal{H} is called a reproducing kernel Hilbert space (RKHS).

We recall that in Theorem 1 of Section 4, the excess risk is decomposed into three terms. In this section, we will detailedly show the corresponding bounds for these three terms and finally put them together to prove our main result (i.e., Theorem 7).

For the first term, we directly cite the following existing theorem:

Theorem 3 (Upper bound on the SNIS bias (Agapiou et al., 2017)). *Assume Assumptions 1–3 hold. Let $\chi^2(Q_t \| P_t)$ denote the χ^2 divergence between Q_t and P_t . Then*

$$\sup_{\|f\|_{\infty} \leq B} \left| \mathbb{E}_{x' \sim P_t} \left[\sum_{j=1}^{N_2} \frac{w_t(x'_j)}{\sum_{j=1}^{N_2} w_t(x'_j)} f(x'_j) \right] - \mathbb{E}_{y \sim Q_t} f(y) \right| \leq \frac{12B(\chi^2(Q_t \| P_t) + 1)}{N_2}. \quad (32)$$

For the second term, we first need a lemma to ensure Lipschitzity of the SNIS statistics:

Lemma 1. *Assume Assumptions 1–4 hold. Let $F_t(X) = \sum_{j=1}^{N_2} \frac{w_t(x_j)}{\sum_{j=1}^{N_2} w_t(x_j)} f(x_j)$ with $X = (x_1, \dots, x_{N_2}) \in \mathbb{R}^{N_2 \times d}$ and $x_{m+1} = (X_{md+1}, \dots, X_{(m+1)d})$ for $m = 0, 1, \dots, d-1$. Under the concentration condition, say $\left| \frac{\sum_{j=1}^{N_2} w_t(x_j)}{N_2} - \mathbb{E}w_t \right| \leq \frac{1}{2} \mathbb{E}w_t$, $F_t(X)$ is $\sqrt{\frac{40}{N_2}} \frac{B\beta}{\mathbb{E}w_t}$ -Lipschitz.*

Lemma 1. For $s = 1, \dots, d$,

$$\begin{aligned} \frac{\partial F_t}{\partial X_s} &= \frac{\left(\frac{\partial w_t(x_1)}{\partial x_{1,k}} f(x_1) + \frac{\partial f(x_1)}{\partial x_{1,k}} w_t(x_1) \right) \left(\sum_{j=1}^{N_2} w_t(x_j) \right) - \frac{\partial w_t(x_1)}{\partial x_{1,k}} \left(\sum_{j=1}^{N_2} w_t(x_j) f(x_j) \right)}{\left(\sum_{j=1}^{N_2} w_t(x_j) \right)^2} \\ &= \frac{\partial f(x_1)}{\partial x_{1,k}} \frac{w_t(x_1)}{\sum_{j=1}^{N_2} w_t(x_j)} + \frac{\partial w_t(x_1)}{\partial x_{1,k}} \frac{\sum_{j=1}^{N_2} (w_t(x_j)(f(x_1) - f(x_j)))}{\left(\sum_{j=1}^{N_2} w_t(x_j) \right)^2} \\ \Rightarrow \frac{\partial F_t}{\partial x_1} &= \frac{w_t(x_1)}{\sum_{j=1}^{N_2} w_t(x_j)} \nabla f(x_1) + \frac{\sum_{j=1}^{N_2} (w_t(x_j)(f(x_1) - f(x_j)))}{\left(\sum_{j=1}^{N_2} w_t(x_j) \right)^2} \nabla w_t \\ \Rightarrow \left\| \frac{\partial F_t}{\partial x_1} \right\|_2^2 &\leq 2 \frac{w_t^2(x_1)}{\left(\sum_{j=1}^{N_2} w_t(x_j) \right)^2} \|\nabla f(x)\|_2^2 + 2 \left(\frac{\sum_{j=1}^{N_2} (w_t(x_j)(f(x_1) - f(x_j)))}{\left(\sum_{j=1}^{N_2} w_t(x_j) \right)^2} \right)^2 \|\nabla w_t\|_2^2 \\ &\leq 2B^2\beta^2 \frac{1}{\left(\sum_{j=1}^{N_2} w_t(x_j) \right)^2} + 8B^2\beta^2 \frac{1}{\left(\sum_{j=1}^{N_2} w_t(x_j) \right)^2} = \frac{10B^2\beta^2}{\left(\sum_{j=1}^{N_2} w_t(x_j) \right)^2}. \end{aligned}$$

Similarly, we can derive the same upper bounds for x_2, \dots, x_{N_2} . Therefore,

$$\left\| \frac{\partial F_t}{\partial X} \right\|_2^2 = \sum_{j=1}^{N_2} \left\| \frac{\partial F_t}{\partial x_j} \right\|_2^2 \leq \frac{10B^2\beta^2 N_2}{\left(\sum_{j=1}^{N_2} w_t(x_j) \right)^2} = \frac{10B^2\beta^2}{N_2} \left(\frac{N_2}{\sum_{j=1}^{N_2} w_t(x_j)} \right)^2.$$

Under the concentration condition, we can conclude that

$$\left\| \frac{\partial F_t}{\partial X} \right\|_2^2 \leq \frac{10B^2\beta^2}{N_2} \left(\frac{N_2}{\sum_{j=1}^{N_2} w_t(x_j)} \right)^2 \leq \frac{40B^2\beta^2}{N_2(\mathbb{E}w_t)^2} \Rightarrow \|F_t\|_{\text{Lip}} \leq \sqrt{\frac{40}{N_2}} \frac{B\beta}{\mathbb{E}w_t}.$$

□

Then we can show the following bound for the weighted empirical process:

Theorem 4 (Upper bound 1 with smoothness and convexity conditions). *Assume Assumptions 1–5 hold. Let $\varepsilon > 0$. Let $\mathcal{N}_\infty(\varepsilon, \mathcal{F}_D)$ denote the L_∞ ε -covering number of \mathcal{F}_D . Then*

$$\begin{aligned} & \mathbb{P} \left(\sup_{f \in \mathcal{F}_D} \left| \sum_{j=1}^{N_2} \frac{w_t(x'_j)}{\sum_{j=1}^{N_2} w_t(x'_j)} f(x'_j) - \mathbb{E}_{x' \sim P_t} \left[\sum_{j=1}^{N_2} \frac{w_t(x'_j)}{\sum_{j=1}^{N_2} w_t(x'_j)} f(x'_j) \right] \right| > \varepsilon \right) \\ & \leq 2\mathcal{N}_\infty \left(\frac{\varepsilon}{3}, \mathcal{F}_D \right) \exp \left(-\frac{\gamma_t N_2 (\mathbb{E}w_t)^2 \varepsilon^2}{1440B^2\beta^2} \right) + 2 \exp \left(-\frac{N_2 (\mathbb{E}w_t)^2}{2B^2} \right). \end{aligned} \quad (33)$$

Theorem 4. The first step is a straightforward application of the Theorem 3.16 in [Wainwright \(2019\)](#). Assumption 5 imposes the strong log-concavity with parameter γ_t , and Lemma 1 indicates the Lipschitzity with parameter $L = \sqrt{\frac{40}{N_2}} \frac{B\beta}{\mathbb{E}w_t}$. Then

$$\begin{aligned} & \mathbb{P} \left(\left| \sum_{j=1}^{N_2} \frac{w_t(x'_j)}{\sum_{j=1}^{N_2} w_t(x'_j)} f(x'_j) - \mathbb{E}_{x' \sim P_t} \left[\sum_{j=1}^{N_2} \frac{w_t(x'_j)}{\sum_{j=1}^{N_2} w_t(x'_j)} f(x'_j) \right] \right| > \frac{\varepsilon}{3} \underbrace{\left| \frac{\sum_{j=1}^{N_2} w_t(x_j)}{N_2} - \mathbb{E}w_t \right|}_{\text{under this concentration condition}} \leq \frac{1}{2} \mathbb{E}w_t \right) \\ & \leq 2 \exp \left(-\frac{\gamma_t N_2 (\mathbb{E}w_t)^2 \varepsilon^2}{1440B^2\beta^2} \right). \end{aligned}$$

When N_2 is relatively large, this concentration condition holds with probability approaching 1 by the large deviation theories, i.e.

$$\mathbb{P} \left(\left| \frac{\sum_{j=1}^{N_2} w_t(x_j)}{N_2} - \mathbb{E}w_t \right| \leq \frac{\mathbb{E}w_t}{2} \right) > 1 - 2 \exp \left(-\frac{N_2 (\mathbb{E}w_t)^2}{2B^2} \right).$$

Now induce a L_∞ $\frac{\varepsilon}{3}$ -covering $\mathcal{F}_{D, \frac{\varepsilon}{3}}$ of \mathcal{F}_D . Therefore, for every $f \in \mathcal{F}_D$, there exists at least an

$f_0 \in \mathcal{F}_{D, \frac{\varepsilon}{3}}$ such that $\|f - f_0\|_\infty < \frac{\varepsilon}{3}$. In this way,

$$\begin{aligned}
& \left\{ \sup_{f \in \mathcal{F}_D} \left| \sum_{j=1}^{N_2} \frac{w_t(x'_j)}{\sum_{j=1}^{N_2} w_t(x'_j)} f(x'_j) - \mathbb{E}_{x' \sim P_t} \left[\sum_{j=1}^{N_2} \frac{w_t(x'_j)}{\sum_{j=1}^{N_2} w_t(x'_j)} f(x'_j) \right] \right| > \varepsilon \right\} \\
&= \left\{ \exists f \in \mathcal{F}_D : \left| \sum_{j=1}^{N_2} \frac{w_t(x'_j)}{\sum_{j=1}^{N_2} w_t(x'_j)} f(x'_j) - \mathbb{E}_{x' \sim P_t} \left[\sum_{j=1}^{N_2} \frac{w_t(x'_j)}{\sum_{j=1}^{N_2} w_t(x'_j)} f(x'_j) \right] \right| > \varepsilon \right\} \\
&\subset \left\{ \exists f \in \mathcal{F}_D, f_0 \in \mathcal{F}_{D, \frac{\varepsilon}{3}} : \left| \sum_{j=1}^{N_2} \frac{w_t(x'_j)}{\sum_{j=1}^{N_2} w_t(x'_j)} (f - f_0)(x'_j) \right| \right. \\
&\quad \left. + \left| \sum_{j=1}^{N_2} \frac{w_t(x'_j)}{\sum_{j=1}^{N_2} w_t(x'_j)} f_0(x'_j) - \mathbb{E}_{x' \sim P_t} \left[\sum_{j=1}^{N_2} \frac{w_t(x'_j)}{\sum_{j=1}^{N_2} w_t(x'_j)} f_0(x'_j) \right] \right| \right. \\
&\quad \left. + \left| \mathbb{E}_{x' \sim P_t} \left[\sum_{j=1}^{N_2} \frac{w_t(x'_j)}{\sum_{j=1}^{N_2} w_t(x'_j)} (f_0 - f)(x'_j) \right] \right| > \varepsilon \right\} \\
&\subset \left\{ \exists f \in \mathcal{F}_D, f_0 \in \mathcal{F}_{D, \frac{\varepsilon}{3}} : \frac{\varepsilon}{3} + \left| \sum_{j=1}^{N_2} \frac{w_t(x'_j)}{\sum_{j=1}^{N_2} w_t(x'_j)} f_0(x'_j) - \mathbb{E}_{x' \sim P_t} \left[\sum_{j=1}^{N_2} \frac{w_t(x'_j)}{\sum_{j=1}^{N_2} w_t(x'_j)} f_0(x'_j) \right] \right| + \frac{\varepsilon}{3} > \varepsilon \right\} \\
&= \left\{ \exists f_0 \in \mathcal{F}_{D, \frac{\varepsilon}{3}} : \left| \sum_{j=1}^{N_2} \frac{w_t(x'_j)}{\sum_{j=1}^{N_2} w_t(x'_j)} f_0(x'_j) - \mathbb{E}_{x' \sim P_t} \left[\sum_{j=1}^{N_2} \frac{w_t(x'_j)}{\sum_{j=1}^{N_2} w_t(x'_j)} f_0(x'_j) \right] \right| > \frac{\varepsilon}{3} \right\}.
\end{aligned}$$

That's to say,

$$\begin{aligned}
& \mathbb{P} \left(\sup_{f \in \mathcal{F}_D} \left| \sum_{j=1}^{N_2} \frac{w_t(x'_j)}{\sum_{j=1}^{N_2} w_t(x'_j)} f(x'_j) - \mathbb{E}_{x' \sim P_t} \left[\sum_{j=1}^{N_2} \frac{w_t(x'_j)}{\sum_{j=1}^{N_2} w_t(x'_j)} f(x'_j) \right] \right| > \varepsilon \right) \\
&\leq \mathbb{P} \left(\sup_{f \in \mathcal{F}_{D, \frac{\varepsilon}{3}}} \left| \sum_{j=1}^{N_2} \frac{w_t(x'_j)}{\sum_{j=1}^{N_2} w_t(x'_j)} f(x'_j) - \mathbb{E}_{x' \sim P_t} \left[\sum_{j=1}^{N_2} \frac{w_t(x'_j)}{\sum_{j=1}^{N_2} w_t(x'_j)} f(x'_j) \right] \right| > \frac{\varepsilon}{3} \right) \\
&\leq \mathbb{P} \left(\sup_{f \in \mathcal{F}_{D, \frac{\varepsilon}{3}}} \left| \sum_{j=1}^{N_2} \frac{w_t(x'_j)}{\sum_{j=1}^{N_2} w_t(x'_j)} f(x'_j) - \mathbb{E}_{x' \sim P_t} \left[\sum_{j=1}^{N_2} \frac{w_t(x'_j)}{\sum_{j=1}^{N_2} w_t(x'_j)} f(x'_j) \right] \right| > \frac{\varepsilon}{3}, \left| \frac{\sum_{j=1}^{N_2} w_t(x_j)}{N_2} - \mathbb{E} w_t \right| \leq \frac{1}{2} \mathbb{E} w_t \right) \\
&\quad + \mathbb{P} \left(\left| \frac{\sum_{j=1}^{N_2} w_t(x_j)}{N_2} - \mathbb{E} w_t \right| > \frac{1}{2} \mathbb{E} w_t \right) \\
&\leq \underbrace{\mathbb{P} \left(\sup_{f \in \mathcal{F}_{D, \frac{\varepsilon}{3}}} \left| \sum_{j=1}^{N_2} \frac{w_t(x'_j)}{\sum_{j=1}^{N_2} w_t(x'_j)} f(x'_j) - \mathbb{E}_{x' \sim P_t} \left[\sum_{j=1}^{N_2} \frac{w_t(x'_j)}{\sum_{j=1}^{N_2} w_t(x'_j)} f(x'_j) \right] \right| > \frac{\varepsilon}{3} \mid \left| \frac{\sum_{j=1}^{N_2} w_t(x_j)}{N_2} - \mathbb{E} w_t \right| \leq \frac{1}{2} \mathbb{E} w_t \right)}_{\text{conditional probability, } \mathbb{P}(A|B) \geq \mathbb{P}(A|B)\mathbb{P}(B) = \mathbb{P}(A, B)} \\
&\quad + \mathbb{P} \left(\left| \frac{\sum_{j=1}^{N_2} w_t(x_j)}{N_2} - \mathbb{E} w_t \right| > \frac{1}{2} \mathbb{E} w_t \right) \\
&\leq 2\mathcal{N}_\infty \left(\frac{\varepsilon}{3}, \mathcal{F}_D \right) \exp \left(-\frac{\gamma_t N_2 (\mathbb{E} w_t)^2 \varepsilon^2}{1440 B^2 \beta^2} \right) + 2 \exp \left(-\frac{N_2 (\mathbb{E} w_t)^2}{2B^2} \right).
\end{aligned}$$

where the last inequality holds by the union bound and Hoeffding's inequality. \square

We can also replace assumption 5 with the following assumption, which imposes convexity on the discriminator space \mathcal{F}_D , not on the distribution P_t :

Assumption 7 (Convexity). *All test functions in \mathcal{F}_D are convex.*

Theorem 5 (Upper bound 2 with smoothness and convexity conditions). *Assume Assumptions 1–4 and 7 hold. Then equation 33 also holds by substituting γ_t with 2. What's more, this substitution holds for all following equations including the term γ_t .*

Theorem 5. Use the Theorem 3.24 in [Wainwright \(2019\)](#) to replace the Theorem 3.16 in the first step of the proof in Theorem 4. Then the remaining argument is completely similar. \square

Theorems 4 and 5 are very standard results for the empirical process theories, except for an extra convergence rate of the concentration condition. Without assumptions 4 and 5, we can also show the following convergence rate:

Theorem 6 (Upper bound without smoothness and convexity conditions). *Assume Assumptions 1–3 hold. Other notations keep the same as before. Then*

$$\begin{aligned} & \mathbb{P} \left(\sup_{f \in \mathcal{F}_D} \left| \sum_{j=1}^{N_2} \frac{w_t(x'_j)}{\sum_{j=1}^{N_2} w_t(x'_j)} f(x'_j) - \mathbb{E}_{x' \sim P_t} \left[\sum_{j=1}^{N_2} \frac{w_t(x'_j)}{\sum_{j=1}^{N_2} w_t(x'_j)} f(x'_j) \right] \right| > \varepsilon \right) \\ & \leq \mathcal{N}_\infty \left(\frac{\varepsilon}{3}, \mathcal{F}_D \right) \frac{36B^2(\chi^2(Q_t \| P_t) + 1)}{N_2 \varepsilon^2}. \end{aligned} \quad (34)$$

Theorem 6. By Theorem 2.1 in Agapiou et al. (2017),

$$\sup_{\|f\|_\infty \leq B} \mathbb{E} \left(\sum_{j=1}^{N_2} \frac{w_t(x'_j)}{\sum_{j=1}^{N_2} w_t(x'_j)} f(x'_j) - \mathbb{E}_{y \sim Q_t} f(y) \right)^2 \leq \frac{4B^2(\chi^2(Q_t \| P_t) + 1)}{N_2}.$$

Thus, for any $f \in \mathcal{F}$, by Markov's inequality,

$$\mathbb{P} \left(\left| \sum_{j=1}^{N_2} \frac{w_t(x'_j)}{\sum_{j=1}^{N_2} w_t(x'_j)} f(x'_j) - \mathbb{E}_{y \sim Q_t} f(y) \right| > \frac{\varepsilon}{3} \right) \leq \frac{36B^2(\chi^2(Q_t \| P_t) + 1)}{N_2 \varepsilon^2}.$$

Then by inducing an L_∞ $\frac{\varepsilon}{3}$ -covering of \mathcal{F}_D we can get the desired result. \square

We can find this rate is much slower than that in equation 33, as mentioned in Section 4, but the convergence still holds.

The third term represents the empirical process of our target function, so by the uniform law of large numbers (e.g., Theorem 9.1 in Györfi et al. (2002)),

$$\mathbb{P} \left(\sup_{h \in \mathcal{F}_D \circ \mathcal{G}_t} \left| \frac{1}{N_1} \sum_{i=1}^{N_1} h(x_i) - \mathbb{E}_{x \sim \hat{P}_t} h(x) \right| > \varepsilon \right) \leq 8 \mathbb{E}_{X \sim \hat{P}_t} \mathcal{N}_1 \left(\frac{\varepsilon}{8}, \mathcal{F}_D \circ \mathcal{G}_t, X^{1:N_1} \right) \exp \left(-\frac{N_1 \varepsilon^2}{512B^2} \right), \quad (35)$$

where $\mathcal{N}_1(\frac{\varepsilon}{8}, \mathcal{F}_D \circ \mathcal{G}_t, X^{1:N_1})$ is the empirical l_1 $\frac{\varepsilon}{8}$ -covering number for the function space $\mathcal{F}_D \circ \mathcal{G}_t := \{f \circ g : f \in \mathcal{F}_D, g \in \mathcal{G}_t\}$ with the empirical l_1 metric $\|f\|_1^{N_1} := \frac{1}{N_1} \sum_{j=1}^{N_1} |f(x_j)|$.

Now we are all set for the proofs of the final bound in Theorem 2, and the following Theorem 7 is a complete and detailed version of Theorem 2.

Theorem 7 (Upper bound on the excess risk). *Assume Assumptions 1–5 hold. Let $\varepsilon > 0$ and $\chi^2(Q_t \| P_t)$ denote the χ^2 divergence between Q_t and P_t . Let $\mathcal{N}_k(\varepsilon, \cdot)$ denote the L_k ε -covering number of a Banach space and $\mathcal{N}'_k(\varepsilon, \cdot, X^{1:n})$ denote the empirical l_k ε -covering number with the empirical l_k metric. Other notations remain the same. Then*

$$\begin{aligned} & \mathbb{P} \left(\sup_{G_t \in \mathcal{G}_t} \left| \text{MMD}(G_t \# \hat{P}_t \| Q_t) - \widehat{\text{MMD}}(G_t \# \hat{P}_t \| Q_t) \right| > \varepsilon + \frac{12B(\chi^2(Q_t \| P_t) + 1)}{N_2} \right) \\ & \leq 2 \mathcal{N}_\infty \left(\frac{\varepsilon}{6}, \mathcal{F}_D \right) \exp \left(-\frac{\gamma_t N_2 (\mathbb{E} w_t)^2 \varepsilon^2}{5760 B^2 \beta^2} \right) + 2 \exp \left(-\frac{N_2 (\mathbb{E} w_t)^2}{2B^2} \right) \\ & \quad + 8 \mathbb{E}_{X \sim \hat{P}_t} \mathcal{N}_1 \left(\frac{\varepsilon}{16}, \mathcal{F}_D \circ \mathcal{G}_t, X^{1:N_1} \right) \exp \left(-\frac{N_1 \varepsilon^2}{2048 B^2} \right) \\ & \leq 2 \mathcal{N}_\infty \left(\frac{\varepsilon}{6}, \mathcal{F}_D \right) \exp \left(-\frac{\gamma_t N_2 (\mathbb{E} w_t)^2 \varepsilon^2}{5760 B^2 \beta^2} \right) + 2 \exp \left(-\frac{N_2 (\mathbb{E} w_t)^2}{2B^2} \right) \\ & \quad + 8 \mathcal{N}_\infty \left(\frac{\varepsilon}{32}, \mathcal{F}_D \right) \mathbb{E}_{X \sim \hat{P}_t} \mathcal{N}_1 \left(\frac{\varepsilon}{32\beta}, \mathcal{G}_t, X^{1:N_1} \right) \exp \left(-\frac{N_1 \varepsilon^2}{2048 B^2} \right). \end{aligned} \quad (36)$$

In other words, for any $\delta > 0$, with probability at least $1 - \delta$, the following inequality holds simultaneously

and uniformly for all $\hat{Q}_t = G_{t\#}\hat{P}_t \in \mathcal{G}_{t\#}\hat{P}_t$ when $N_1 \geq N_1(\delta)$ and $N_2 \geq N_2(\delta)$:

$$\begin{aligned} \text{MMD}(\hat{Q}_t \| Q_t) &\leq \widehat{\text{MMD}}(\hat{Q}_t \| Q_t) \\ &+ \frac{12B(\chi^2(Q_t \| P_t) + 1)}{N_2} + \left(\frac{64B\beta}{\sqrt{\gamma_t}(\mathbb{E}w_t)} \sqrt{\frac{\log \mathcal{N}_\infty(\frac{\varepsilon(\delta)}{6}, \mathcal{F}_D)}{N_2}} + 64B \sqrt{\frac{\log \mathcal{N}_\infty(\frac{\varepsilon(\delta)}{32}, \mathcal{F}_D) + \log \mathbb{E} \mathcal{N}_1(\frac{\varepsilon(\delta)}{32\beta}, \mathcal{G}_t, X^{1:N_1})}{N_1}} \right) \sqrt{\log \frac{3}{\delta}}. \end{aligned} \quad (37)$$

This further implies

$$\begin{aligned} \underbrace{\text{MMD}(\hat{G}_{t\#}\hat{P}_t \| Q_t)}_{\text{empirical estimate}} &\leq \underbrace{\inf_{G_t \in \mathcal{G}_t} \text{MMD}(G_{t\#}\hat{P}_t \| Q_t)}_{\text{the best estimate}} \\ &+ \frac{24B(\chi^2(Q_t \| P_t) + 1)}{N_2} + \left(\frac{128B\beta}{\sqrt{\gamma_t}(\mathbb{E}w_t)} \sqrt{\frac{\log \mathcal{N}_\infty(\mathcal{F}_D)}{N_2}} + 128B \sqrt{\frac{\log \mathcal{N}_\infty(\mathcal{F}_D) + \log \mathbb{E} \mathcal{N}_1^\beta(\mathcal{G}_t)}{N_1}} \right) \sqrt{\log \frac{3}{\delta}}, \end{aligned} \quad (38)$$

where $\mathcal{N}_\infty(\mathcal{F}_D)$ and $\mathcal{N}_1^\beta(\mathcal{G}_t)$ are short for the corresponding terms.

Theorem 7. The first inequality in equation 36 holds by combining Theorem 1, Theorem 4, and equation 35 together:

$$\begin{aligned} &\mathbb{P} \left(\sup_{G_t \in \mathcal{G}_t} \left| \text{MMD}(G_{t\#}\hat{P}_t \| Q_t) - \widehat{\text{MMD}}(G_{t\#}\hat{P}_t \| Q_t) \right| > \varepsilon + \frac{12B(\chi^2(Q_t \| P_t) + 1)}{N_2} \right) \\ &\leq \mathbb{P} \left(\sup_{f \in \mathcal{F}_D} \left| \mathbb{E}_{y \sim Q_t} f(y) - \mathbb{E}_{x' \sim P_t} \left[\sum_{j=1}^{N_2} \frac{w_t(x'_j)}{\sum_{j=1}^{N_2} w_t(x'_j)} f(x'_j) \right] \right| \right. \\ &\quad \left. + \sup_{f \in \mathcal{F}_D} \left| \mathbb{E}_{x' \sim P_t} \left[\sum_{j=1}^{N_2} \frac{w_t(x'_j)}{\sum_{j=1}^{N_2} w_t(x'_j)} f(x'_j) \right] - \sum_{j=1}^{N_2} \frac{w_t(x'_j)}{\sum_{j=1}^{N_2} w_t(x'_j)} f(x'_j) \right| \right. \\ &\quad \left. + \sup_{h \in \mathcal{F}_D \circ \mathcal{G}_t} \left| \frac{1}{N_1} \sum_{i=1}^{N_1} h(x_i) - \mathbb{E}_{x \sim \hat{P}_t} h(x) \right| > \frac{12B(\chi^2(Q_t \| P_t) + 1)}{N_2} + \frac{\varepsilon}{2} + \frac{\varepsilon}{2} \right) \\ &\leq \mathbb{P} \left(\sup_{f \in \mathcal{F}_D} \left| \mathbb{E}_{x' \sim P_t} \left[\sum_{j=1}^{N_2} \frac{w_t(x'_j)}{\sum_{j=1}^{N_2} w_t(x'_j)} f(x'_j) \right] - \sum_{j=1}^{N_2} \frac{w_t(x'_j)}{\sum_{j=1}^{N_2} w_t(x'_j)} f(x'_j) \right| > \frac{12B(\chi^2(Q_t \| P_t) + 1)}{N_2} \right) \\ &\quad + \mathbb{P} \left(\sup_{f \in \mathcal{F}_D} \left| \mathbb{E}_{x' \sim P_t} \left[\sum_{j=1}^{N_2} \frac{w_t(x'_j)}{\sum_{j=1}^{N_2} w_t(x'_j)} f(x'_j) \right] - \sum_{j=1}^{N_2} \frac{w_t(x'_j)}{\sum_{j=1}^{N_2} w_t(x'_j)} f(x'_j) \right| > \frac{\varepsilon}{2} \right) \\ &\quad + \mathbb{P} \left(\sup_{h \in \mathcal{F}_D \circ \mathcal{G}_t} \left| \frac{1}{N_1} \sum_{i=1}^{N_1} h(x_i) - \mathbb{E}_{x \sim \hat{P}_t} h(x) \right| > \frac{\varepsilon}{2} \right) \\ &\leq 0 + 2\mathcal{N}_\infty \left(\frac{\varepsilon}{6}, \mathcal{F}_D \right) \exp \left(-\frac{\gamma_t N_2 (\mathbb{E}w_t)^2 \varepsilon^2}{5760 B^2 \beta^2} \right) + 2 \exp \left(-\frac{N_2 (\mathbb{E}w_t)^2}{2B^2} \right) \\ &\quad + 8\mathbb{E}_{X \sim \hat{P}_t} \mathcal{N}_1 \left(\frac{\varepsilon}{16}, \mathcal{F}_D \circ \mathcal{G}_t, X^{1:N_1} \right) \exp \left(-\frac{N_1 \varepsilon^2}{2048 B^2} \right). \end{aligned}$$

For the second inequality, we can induce an $L_\infty \frac{\varepsilon}{32}$ -covering of \mathcal{F}_D and an empirical $L_1 \frac{\varepsilon}{32\beta} \|\cdot\|_2$ covering of \mathcal{G}_t . For every $f \in \mathcal{F}_D$ and $g \in \mathcal{G}_t$, there exist an $\tilde{f} \in \mathcal{F}_{\frac{\varepsilon}{32}}$ and a $\tilde{g} \in \mathcal{G}_{t, \frac{\varepsilon}{32\beta}}$ such that

$\|f - \tilde{f}\|_\infty < \frac{\varepsilon}{32}$ and $\frac{1}{N_1} \sum_{i=1}^{N_1} \|g(x_i) - \tilde{g}(x_i)\|_2 < \frac{\varepsilon}{32\beta}$. Then by the Lipschitz assumption,

$$\begin{aligned} \frac{1}{N_1} \sum_{i=1}^{N_1} f(g(x_i)) &\leq \frac{1}{N_1} \sum_{i=1}^{N_1} [f(\tilde{g}(x_i)) + \beta \|g(x_i) - \tilde{g}(x_i)\|_2] \\ &\leq \frac{1}{N_1} \sum_{i=1}^{N_1} f(\tilde{g}(x_i)) + \frac{\varepsilon}{32} \\ &\leq \frac{1}{N_1} \sum_{i=1}^{N_1} \tilde{f}(\tilde{g}(x_i)) + \frac{\varepsilon}{16}. \end{aligned}$$

Similarly, $\frac{1}{N_1} \sum_{i=1}^{N_1} \tilde{f}(\tilde{g}(x_i)) - \frac{\varepsilon}{16} \leq \frac{1}{N_1} \sum_{i=1}^{N_1} f(g(x_i))$. Thus,

$$\mathbb{E}_{X \sim \hat{P}_t} \mathcal{N}_1 \left(\frac{\varepsilon}{16}, \mathcal{F}_D \circ \mathcal{G}_t, X^{1:N_1} \right) \leq \mathcal{N}_\infty \left(\frac{\varepsilon}{32}, \mathcal{F}_D \right) \mathbb{E}_{X \sim \hat{P}_t} \mathcal{N}_1 \left(\frac{\varepsilon}{32\beta}, \mathcal{G}_t, X^{1:N_1} \right).$$

For the third inequality, let $\varepsilon = \varepsilon(\delta)$ be the solution of

$$\varepsilon = \left(\frac{64B\beta}{\sqrt{\gamma_t}(\mathbb{E}w_t)} \sqrt{\frac{\log \mathcal{N}_\infty(\frac{\varepsilon}{6}, \mathcal{F}_D)}{N_2}} + 64B \sqrt{\frac{\log \mathcal{N}_\infty(\frac{\varepsilon}{32}, \mathcal{F}_D) + \log \mathbb{E} \mathcal{N}_1(\frac{\varepsilon}{32\beta}, \mathcal{G}_t, X^{1:N_1})}{N_1}} \right) \sqrt{\log \frac{3}{\delta}}. \quad (39)$$

Since the left-hand side is an increasing function with regard to ε while the right-hand side is a decreasing one, this equation will consistently have exactly one solution for any N_1, N_2 and δ . By plugging this equation into the second inequality and letting N_2 be large enough such that $2 \exp\left(-\frac{N_2(\mathbb{E}w_t)^2}{2B^2}\right) < \frac{\delta}{3}$, we can immediately derive the third inequality.

For the last inequality, use the definition of \hat{G}_t :

$$\begin{aligned} \text{MMD}(\hat{G}_t \# \hat{P}_t \| Q_t) &\leq \widehat{\text{MMD}}(\hat{G}_t \# \hat{P}_t \| Q_t) + \text{excess_term} \\ &\leq \inf_{G_t \in \mathcal{G}_t} \widehat{\text{MMD}}(G_t \# \hat{P}_t \| Q_t) + \text{excess_term} \\ &\leq \inf_{G_t \in \mathcal{G}_t} \text{MMD}(G_t \# \hat{P}_t \| Q_t) + 2 \times \text{excess_term}. \end{aligned}$$

□

Proposition 1.

$$\begin{aligned} d_{\mathcal{F}_D}(P \| Q) &= \sup_{f \in \mathcal{F}_D} |\mathbb{E}_{x \sim P} f(x) - \mathbb{E}_{y \sim Q} f(y)| = \sup_{\|f\|_{\mathcal{H}} \leq 1} |\mathbb{E}_{x \sim P} f(x) - \mathbb{E}_{y \sim Q} f(y)|^2 \\ &= \sup_{\|f\|_{\mathcal{H}} \leq 1} |\mathbb{E}_{x \sim P} \langle f, \phi(x) \rangle_{\mathcal{H}} - \mathbb{E}_{y \sim Q} \langle f, \phi(y) \rangle_{\mathcal{H}}|^2 \\ &= \sup_{\|f\|_{\mathcal{H}} \leq 1} |\langle f, [\mathbb{E}_{x \sim P} \phi(G_t(x)) - \mathbb{E}_{y \sim Q} \phi(y)] \rangle_{\mathcal{H}}|^2 \\ &= \|\mathbb{E}_{x \sim P} \phi(x) - \mathbb{E}_{y \sim Q} \phi(y)\|_{\mathcal{H}}^2 \quad \left(\text{since } f^* = \frac{\mathbb{E}_{x \sim P} \phi(x) - \mathbb{E}_{y \sim Q} \phi(y)}{\|\mathbb{E}_{x \sim P} \phi(x) - \mathbb{E}_{y \sim Q} \phi(y)\|_{\mathcal{H}}} \right) \\ &= \mathbb{E}_{x, x' \sim P} K(x, x') - 2\mathbb{E}_{x \sim P, y \sim Q} K(G_t(x), y) + \mathbb{E}_{y \sim Q, y' \sim Q} K(y, y'). \end{aligned}$$

□

Theorem 1. All following inequalities are directly derived by the absolute value inequality, i.e., $|a| + |b| \geq$

$|a + b|$.

$$\begin{aligned}
& \text{MMD}(\hat{Q}_t \| Q_t) - \widehat{\text{MMD}}(\hat{Q}_t \| Q_t) \\
&= \sup_{f \in \mathcal{F}_D} \left| \mathbb{E}_{x \sim \hat{P}_t} f(G_t(x)) - \mathbb{E}_{x' \sim Q_t} f(x') \right| - \sup_{f \in \mathcal{F}_D} \left| \frac{1}{N_1} \sum_{i=1}^{N_1} f(G_t(x_i)) - \sum_{j=1}^{N_2} \frac{w_t(x'_j)}{\sum_{j=1}^{N_2} w_t(x'_j)} f(x'_j) \right| \\
&\leq \sup_{f \in \mathcal{F}_D} \left| \mathbb{E}_{y \sim Q_t} f(y) - \sum_{j=1}^{N_2} \frac{w_t(x'_j)}{\sum_{j=1}^{N_2} w_t(x'_j)} f(x'_j) \right| + \sup_{f \in \mathcal{F}_D} \left| \frac{1}{N_1} \sum_{i=1}^{N_1} f(G_t(x_i)) - \mathbb{E}_{x \sim \hat{P}_t} f(G_t(x)) \right| \\
&\leq \sup_{f \in \mathcal{F}_D} \left| \mathbb{E}_{y \sim Q_t} f(y) - \mathbb{E}_{x' \sim P_t} \left[\sum_{j=1}^{N_2} \frac{w_t(x'_j)}{\sum_{j=1}^{N_2} w_t(x'_j)} f(x'_j) \right] \right| \\
&\quad + \left| \mathbb{E}_{x' \sim P_t} \left[\sum_{j=1}^{N_2} \frac{w_t(x'_j)}{\sum_{j=1}^{N_2} w_t(x'_j)} f(x'_j) \right] - \sum_{j=1}^{N_2} \frac{w_t(x'_j)}{\sum_{j=1}^{N_2} w_t(x'_j)} f(x'_j) \right| \\
&\quad + \sup_{h \in \mathcal{F}_D \circ \mathcal{G}_t} \left| \frac{1}{N_1} \sum_{i=1}^{N_1} h(x_i) - \mathbb{E}_{x \sim \hat{P}_t} h(x) \right|.
\end{aligned}$$

□

Proposition 2. Consider an optimal coupling between \hat{Q}_t and Q_t and denote it as $\Gamma(\hat{Q}_t, Q_t)$. The corresponding marginals are denoted as \tilde{Q}_t and \tilde{Q}_t , respectively. Note that $\tilde{Q}_t \stackrel{d}{=} \hat{Q}_t$ and $\tilde{Q}_t \stackrel{d}{=} Q_t$. Then by the definition,

$$\begin{aligned}
& \text{MMD}(\mathcal{M}_t(\hat{Q}_t) + p_{\eta_{t+1}} \| \mathcal{M}_t(Q_t) + p_{\eta_{t+1}}) \\
&= \sup_{f \in \mathcal{F}_D} \left| \mathbb{E}_{X \sim \hat{Q}_t, \eta_{t+1}^1 \sim p_{\eta_{t+1}}} f(\mathcal{M}_t(X) + \eta_{t+1}^1) - \mathbb{E}_{Y \sim Q_t, \eta_{t+1}^2 \sim p_{\eta_{t+1}}} f(\mathcal{M}_t(Y) + \eta_{t+1}^2) \right| \\
&= \sup_{f \in \mathcal{F}_D} \left| \mathbb{E}_{X \sim \tilde{Q}_t, \eta_{t+1} \sim p_{\eta_{t+1}}} f(\mathcal{M}_t(X) + \eta_{t+1}) - \mathbb{E}_{Y \sim \tilde{Q}_t, \eta_{t+1} \sim p_{\eta_{t+1}}} f(\mathcal{M}_t(Y) + \eta_{t+1}) \right| \\
&= \sup_{f \in \mathcal{F}_D} \left| \mathbb{E}_{X \sim \tilde{Q}_t, Y \sim \tilde{Q}_t, \eta_{t+1} \sim p_{\eta_{t+1}}} f(\mathcal{M}_t(Y) + \eta_{t+1} + (\mathcal{M}_t(X) - \mathcal{M}_t(Y))) - \mathbb{E}_{Y \sim \tilde{Q}_t, \eta_{t+1} \sim p_{\eta_{t+1}}} f(\mathcal{M}_t(Y) + \eta_{t+1}) \right| \\
&\leq \underbrace{\sup_{f \in \mathcal{F}_D} \left| \mathbb{E}_{X \sim \tilde{Q}_t, Y \sim \tilde{Q}_t, \eta_{t+1} \sim p_{\eta_{t+1}}} f(\mathcal{M}_t(Y) + \eta_{t+1}) - \mathbb{E}_{Y \sim \tilde{Q}_t, \eta_{t+1} \sim p_{\eta_{t+1}}} f(\mathcal{M}_t(Y) + \eta_{t+1}) \right|}_{=0} \\
&\quad + \beta \mathbb{E}_{X \sim \tilde{Q}_t, Y \sim \tilde{Q}_t} \|\mathcal{M}_t(X) - \mathcal{M}_t(Y)\|_2 \quad (\text{by Lipschitzity of } f) \\
&\leq \beta \gamma \mathbb{E}_{X \sim \tilde{Q}_t, Y \sim \tilde{Q}_t} \|X - Y\|_2 \quad (\text{by Lipschitzity of } \mathcal{M}_t) \\
&\leq \beta \gamma \left(\mathbb{E}_{X, Y \sim \Gamma(\hat{Q}_t, Q_t)} \|X - Y\|_2^2 \right)^{\frac{1}{2}} \quad (\text{by Cauchy's inequality}) \\
&= W_2(\hat{Q}_t \| Q_t).
\end{aligned}$$

□

Proposition 3. By the definition,

$$\begin{aligned}
& \text{MMD}(\mathcal{M}_t(\hat{Q}_t) + p_{\eta_{t+1}} \| \mathcal{M}_t(Q_t) + p_{\eta_{t+1}}) \\
&= \sup_{\|f\|_{\mathcal{H}} \leq 1} \left| \mathbb{E}_{X \sim \hat{Q}_t, \eta_{t+1}^1 \sim p_{\eta_{t+1}}} f(\mathcal{M}_t(X) + \eta_{t+1}^1) - \mathbb{E}_{Y \sim Q_t, \eta_{t+1}^2 \sim p_{\eta_{t+1}}} f(\mathcal{M}_t(Y) + \eta_{t+1}^2) \right| \\
&\leq \sup_{\|f\|_{\mathcal{H}} \leq 1} \left| \mathbb{E}_{X \sim \hat{Q}_t} f(\mathcal{M}_t(X)) - \mathbb{E}_{Y \sim Q_t} f(\mathcal{M}_t(Y)) \right| + \beta \mathbb{E}_{\eta_{t+1}^1 \sim p_{\eta_{t+1}}} \|\eta_{t+1}^1\| + \beta \mathbb{E}_{\eta_{t+1}^2 \sim p_{\eta_{t+1}}} \|\eta_{t+1}^2\| \\
&\leq \sup_{\|g\|_{\mathcal{H}} \leq \Omega} \left| \mathbb{E}_{X \sim \hat{Q}_t} g(X) - \mathbb{E}_{Y \sim Q_t} g(Y) \right| + 2\beta \mathbb{E}_{p_{\eta_{t+1}}} \|\eta_{t+1}\| \quad (g = f \circ \mathcal{M}_t) \\
&\leq \Omega \sup_{\|g\|_{\mathcal{H}} \leq 1} \left| \mathbb{E}_{X \sim \hat{Q}_t} g(X) - \mathbb{E}_{Y \sim Q_t} g(Y) \right| + 2\beta (\mathbb{E}_{p_{\eta_{t+1}}} \|\eta_{t+1}\|_2^2)^{\frac{1}{2}} \\
&= \Omega \cdot \text{MMD}(\hat{Q}_t \| Q_t) + 2\beta \cdot \text{trace}(\text{Var}(\eta_{t+1}))^{\frac{1}{2}}.
\end{aligned}$$

□

Corollary 1. By the sub-Gaussian assumption,

$$\begin{aligned}
\mathbb{P} \left(\exists i \in [N_1], \|X_i\|_{\infty} \geq C_6 \sigma_t \sqrt{\log(2dN_1) + \frac{N_1 \varepsilon^2}{2048B^2}} \right) &\stackrel{\text{union bound}}{\leq} N_1 d \mathbb{P} \left(X_{11} \geq C_6 \sigma_t \sqrt{\log(2dN_1) + \frac{N_1 \varepsilon^2}{2048B^2}} \right) \\
&\stackrel{\text{tail bound}}{\leq} \exp \left(-\frac{N_1 \varepsilon^2}{2048B^2} \right)
\end{aligned}$$

where C_6 is an absolute constant and the term “ $\exp \left(-\frac{N_1 \varepsilon^2}{2048B^2} \right)$ ” matches the nonasymptotic bound on the right-hand side of equation 36. In this way, under the condition

$$\mathcal{A} := \left\{ \max_{1 \leq i \leq N_1} \|X_i\|_{\infty} \leq M := C_6 \sigma_t \sqrt{\log(2dN_1) + \frac{N_1 \varepsilon^2}{2048B^2}} \right\},$$

since the l_1 norm is dominated by the L_{∞} norm,

$$\log \mathbb{E}_{X \sim \hat{P}_t} \mathcal{N}_1 \left(\frac{\varepsilon}{32\beta}, \mathcal{G}_t, X^{1:N_1} \right) \leq \log \mathcal{N}_{\infty} \left(\frac{\varepsilon}{32\beta}, \mathcal{G}_t |_{[-M, M]^d} \right) \quad (40)$$

$$\stackrel{\text{equation 23}}{\leq} 2C_7 SL \log \left(\beta L \|W\|_{\infty} (R \vee 1) \sigma_t \sqrt{\frac{\log(2dN_1)}{\varepsilon^2} + \frac{N_1}{2048B^2}} \right). \quad (41)$$

Therefore,

$$\begin{aligned}
& \mathbb{P} \left(\sup_{G_t \in \mathcal{G}_t} \left| \text{MMD}(G_{t\#} \hat{P}_t \| Q_t) - \widehat{\text{MMD}}(G_{t\#} \hat{P}_t \| Q_t) \right| > \varepsilon + \frac{12B(\chi^2(Q_t \| P_t) + 1)}{N_2} \right) \\
&\leq \mathbb{P} \left(\sup_{G_t \in \mathcal{G}_t} \left| \text{MMD}(G_{t\#} \hat{P}_t \| Q_t) - \widehat{\text{MMD}}(G_{t\#} \hat{P}_t \| Q_t) \right| > \varepsilon + \frac{12B(\chi^2(Q_t \| P_t) + 1)}{N_2}, \mathcal{A} \right) + \mathbb{P}(\mathcal{A}^c) \\
&\leq \mathbb{P} \left(\sup_{G_t \in \mathcal{G}_t} \left| \text{MMD}(G_{t\#} \hat{P}_t \| Q_t) - \widehat{\text{MMD}}(G_{t\#} \hat{P}_t \| Q_t) \right| > \varepsilon + \frac{12B(\chi^2(Q_t \| P_t) + 1)}{N_2} \middle| \mathcal{A} \right) + \exp \left(-\frac{N_1 \varepsilon^2}{2048B^2} \right) \\
&\leq 2\mathcal{N}_{\infty} \left(\frac{\varepsilon}{6}, \mathcal{F}_D \right) \exp \left(-\frac{\gamma_t N_2 (\mathbb{E}w_t)^2 \varepsilon^2}{5760B^2 \beta^2} \right) + 2 \exp \left(-\frac{N_2 (\mathbb{E}w_t)^2}{2B^2} \right) \\
&\quad + 9\mathcal{N}_{\infty} \left(\frac{\varepsilon}{32}, \mathcal{F}_D \right) \mathcal{N}_{\infty} \left(\frac{\varepsilon}{32\beta}, \mathcal{G}_t |_{[-M, M]^d} \right) \exp \left(-\frac{N_1 \varepsilon^2}{2048B^2} \right),
\end{aligned}$$

where the last inequality follows from equation 18 and equation 40. □

Proposition 4. We first prove a lemma.

Lemma 2. Let N be the size of neural networks. Then under assumptions 1-6 and the sub-Gaussian condition, the approximation error will converge at the following rate:

$$\inf_{G_t \in \mathcal{G}_t} \text{MMD}(\hat{Q}_t \| Q_t) \lesssim (\log N)^{\frac{5}{2}} N^{-\frac{5}{d}}. \quad (42)$$

That is, the convergence rate with regard to N in sub-Gaussian cases will be slower by a factor $(\log N)^{\frac{s}{2}}$ than that in bounded cases.

Proof. By bounded, Lipschitzity and sub-Gaussian assumptions,

$$\begin{aligned}
\inf_{G_t \in \mathcal{G}_t} \text{MMD}(\hat{Q}_t \| Q_t) &= \inf_{G_t \in \mathcal{G}_t} \sup_{f \in \mathcal{F}_D} \left| \mathbb{E}_{x \sim G_t \# \hat{P}_t} f(x) - \mathbb{E}_{y \sim Q_t} f(y) \right| \\
&= \inf_{G_t \in \mathcal{G}_t} \sup_{f \in \mathcal{F}_D} \left| \mathbb{E}_{x \sim G_t \# \hat{P}_t} f(x) - \mathbb{E}_{y \sim G'_t \# \hat{P}_t} f(y) \right| \\
&= \inf_{G_t \in \mathcal{G}_t} \sup_{f \in \mathcal{F}_D} \int f(G_t(x)) - f(G'_t(x)) d\hat{P}_t \\
&= \inf_{G_t \in \mathcal{G}_t} \sup_{f \in \mathcal{F}_D} \left(\int_{\|x\|_\infty > H} f(G_t(x)) - f(G'_t(x)) d\hat{P}_t + \int_{\|x\|_\infty \leq H} f(G_t(x)) - f(G'_t(x)) d\hat{P}_t \right) \\
&\lesssim 2B\hat{P}_t(\|x\|_\infty > H) + \inf_{G_t \in \mathcal{G}_t} \beta \int_{\|x\|_\infty \leq H} \|G_t(x) - G'_t(x)\|_2 d\hat{P}_t \\
&\lesssim 2Bd \exp\left(-\frac{H^2}{\sigma_t^2}\right) + \inf_{G_t \in \mathcal{G}_t} \beta \|G_t - G'_t\|_{L_\infty[-H, H]^d}.
\end{aligned}$$

Assume $m \in \mathbb{N}$ satisfies $\frac{d}{p} < s < \min(m, m - 1 + \frac{1}{p})$, $\nu = \frac{s-\delta}{2\delta}$, $\varepsilon = N^{-\frac{s}{d} - (\nu^{-1} + d^{-1})(\frac{d}{p} - s)} + \log(N)^{-1}$, $W_0 = 6dm(m+2) + 2d$, $L = 3 + 2\lceil \log_2(\frac{3^{d\nu m}}{\varepsilon C(d, m)}) + 5 \rceil \lceil \log_2(d \vee m) \rceil$, $W = NW_0$, $S = (L-1)W_0^2 N + N$ and $R = O(N^{(\nu^{-1} + d^{-1})(1 \vee (\frac{d}{p} - s))})$ where N is the number of B-spline functions. By Proposition 1 of Suzuki (2019) and dividing the domain into cubes with each side length 1, the second term has the convergence rate $H^s N^{-\frac{s}{d}}$. Since this inequality holds for all $H \in \mathbb{R}_+$, then by minimizing the right-hand side over H we can find the extra factor $(\log N)^{\frac{s}{2}}$. \square

Then we can derive this proposition simply by (1) using the chaining method (i.e., take expectations on the empirical MMD term of equation 19 in Theorem 2 and apply $\mathbb{E}X = \int_0^{+\infty} \mathbb{P}(X > t) dt$) or referring to Lemma 26 in Liang (2021) (i.e., the standard entropy integral bound) and (2) plugging equation 22 with $\gamma = \frac{1}{d}$ in the second case, equation 24 and equation 42 into the Dudley entropy integral and minimizing the right-hand side over $\delta \in [0, \frac{1}{2}]$ and $N \in \mathbb{Z}_+$. That is,

$$\begin{aligned}
&\mathbb{E} \text{MMD}(\hat{Q}_t \| Q_t) - \inf_{G_t \in \mathcal{G}_t} \text{MMD}(\hat{Q}_t \| Q_t) \\
&\lesssim \inf_{0 < \delta < \frac{1}{2}} \left(4\delta + \frac{8\sqrt{2}}{\sqrt{N_1}} \int_\delta^{\frac{1}{2}} \sqrt{\log \mathcal{N}_\infty(\varepsilon, \mathcal{F}_D) + \log \mathcal{N}_\infty(\frac{\varepsilon}{32\beta}, \mathcal{G}_t|_{[-M, M]^d})} d\varepsilon \right. \\
&\quad \left. + \frac{8\sqrt{2}}{\sqrt{N_2}} \int_\delta^{\frac{1}{2}} \sqrt{\log \mathcal{N}_\infty(\varepsilon, \mathcal{F}_D)} d\varepsilon \right) \\
&\lesssim \inf_{0 < \delta < \frac{1}{2}} \left(4\delta + \frac{8\sqrt{2}}{\sqrt{N_1}} \int_\delta^{\frac{1}{2}} \sqrt{\log \mathcal{N}_\infty(\varepsilon, \mathcal{F}_D)} d\varepsilon + \frac{8\sqrt{2}}{\sqrt{N_1}} \int_\delta^{\frac{1}{2}} \sqrt{\log \mathcal{N}_\infty(\frac{\varepsilon}{32\beta}, \mathcal{G}_t|_{[-M, M]^d})} d\varepsilon \right. \\
&\quad \left. + \frac{8\sqrt{2}}{\sqrt{N_2}} \int_\delta^{\frac{1}{2}} \sqrt{\log \mathcal{N}_\infty(\varepsilon, \mathcal{F}_D)} d\varepsilon \right) \\
&\lesssim \frac{N \log(NN_1)}{\sqrt{N_1}} + \frac{1}{\sqrt{N_2}} \quad (\text{by taking } \delta = 0) \\
&\Rightarrow \mathbb{E} \text{MMD}(\hat{Q}_t \| Q_t) \\
&\lesssim (\log N)^{\frac{s}{2}} N^{-\frac{s}{d}} + \frac{N \log(NN_1)}{\sqrt{N_1}} + \frac{1}{\sqrt{N_2}} \\
&\lesssim (\log N_1)^{\frac{s}{2} \vee 1} N_1^{-\frac{s}{2(s+d)}} + N_2^{-\frac{1}{2}}. \quad (\text{by taking } N \asymp N_1^{\frac{d}{2(s+d)}})
\end{aligned}$$

□

Proposition 5. Under the circumstance of the linear kernel, minimizing the empirical MMD loss is equivalent to minimizing the empirical L_2 loss:

$$\begin{aligned}
\hat{G}_t &= \arg \min_{G_t \in \mathcal{G}_t} \frac{1}{N_1^2} \sum_{i=1}^{N_1} \sum_{j=1}^{N_1} K(G_t(x_i), G_t(x_j)) - \frac{2}{N_1} \sum_{i=1}^{N_1} \sum_{j=1}^{N_2} \underbrace{\frac{w_t(x'_j)}{\sum_{j=1}^{N_2} w_t(x'_j)}}_{:=w_j} K(G_t(x_i), x'_j) \\
&= \arg \min_{G_t \in \mathcal{G}_t} \frac{1}{N_1^2} \sum_{i=1}^{N_1} \sum_{j=1}^{N_1} K(G_t(x_i), G_t(x_j)) - \frac{2}{N_1} \sum_{i=1}^{N_1} \sum_{j=1}^{N_2} w_j K(G_t(x_i), x'_j) + \sum_{i=1}^{N_2} \sum_{j=1}^{N_2} w_i w_j K(x'_i, x'_j) \\
&= \arg \min_{G_t \in \mathcal{G}_t} \left(\frac{\sum_{i=1}^{N_1} G_t(x_i)}{N_1} \right)^T \left(\frac{\sum_{j=1}^{N_1} G_t(x_j)}{N_1} \right) - 2 \left(\frac{\sum_{i=1}^{N_1} G_t(x_i)}{N_1} \right)^T \left(\sum_{j=1}^{N_2} w_j x'_j \right) + \left(\sum_{i=1}^{N_2} w_i x'_i \right)^T \left(\sum_{j=1}^{N_2} w_j x'_j \right) \\
&= \arg \min_{G_t \in \mathcal{G}_t} \left\| \frac{\sum_{i=1}^{N_1} G_t(x_i)}{N_1} - \sum_{j=1}^{N_2} w_j x'_j \right\|_2^2.
\end{aligned}$$

Then by taking the following two steps: (1) mimicking the proofs of Proposition 4 in this paper and (2) plugging equation 22 with $\gamma = d$ in the first case and equation 24 into the Dudley entropy integral, we can derive the desired conclusion. Moreover, the approximation error will be zero (i.e., the term $\inf_{G_t \in \mathcal{G}_t} \text{MMD}(G_t \# \hat{P}_t \| Q_t)$ vanishes) as long as the constant function $h(X) \equiv \mathbb{E}_{Y \sim Q_t} Y$ belongs to the set $\Phi(L, W, S, R)$. For example, let $R \geq \|\mathbb{E}_{Y \sim Q_t} Y\|_\infty$. □

B Supplementary Figures and Tables

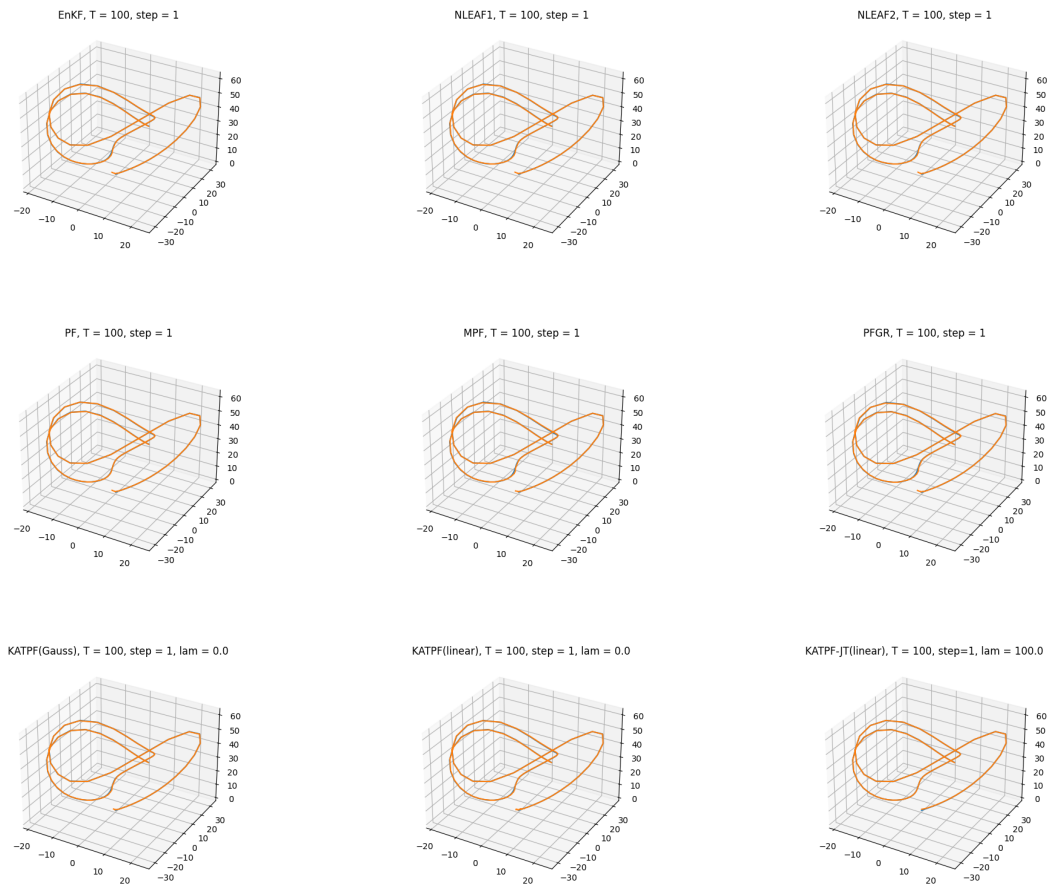


Figure 4: Experimental results of the Lorenz63 system when $T = 100$ and $\Delta t = 0.02$.

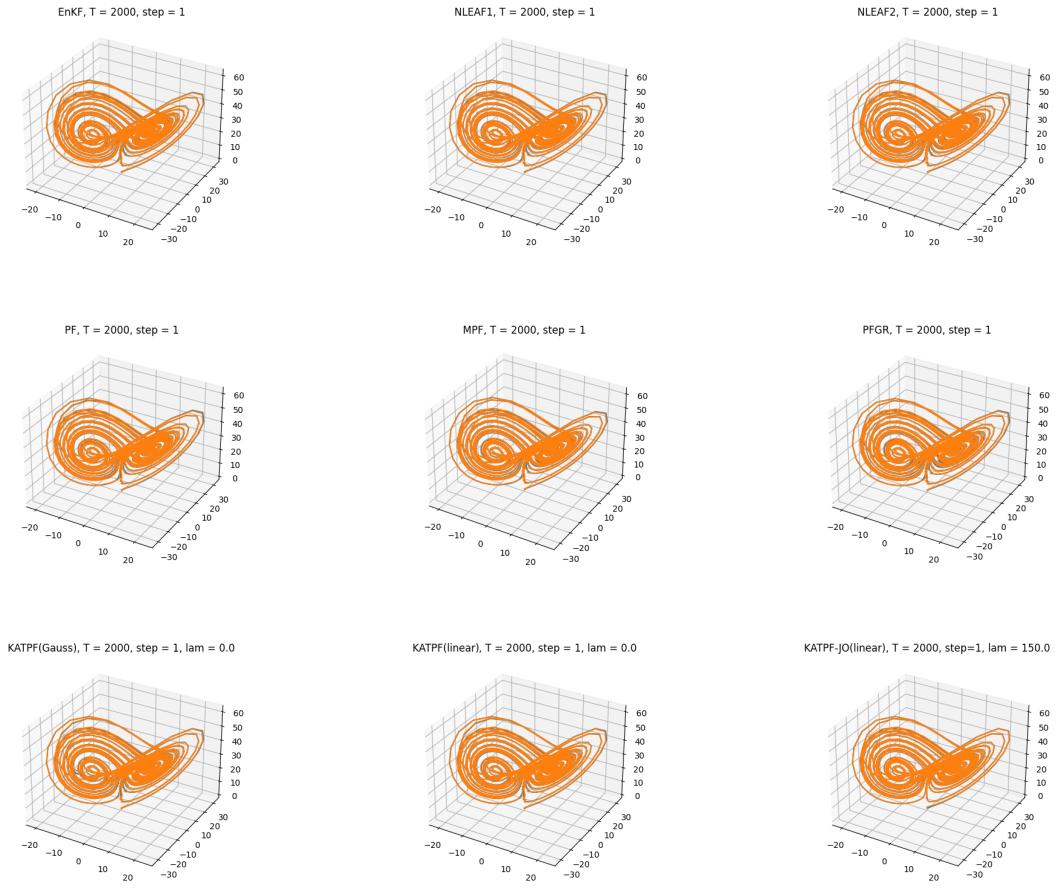


Figure 5: Experimental results of the Lorenz63 system when $T = 2000$ and $\Delta t = 0.02$.

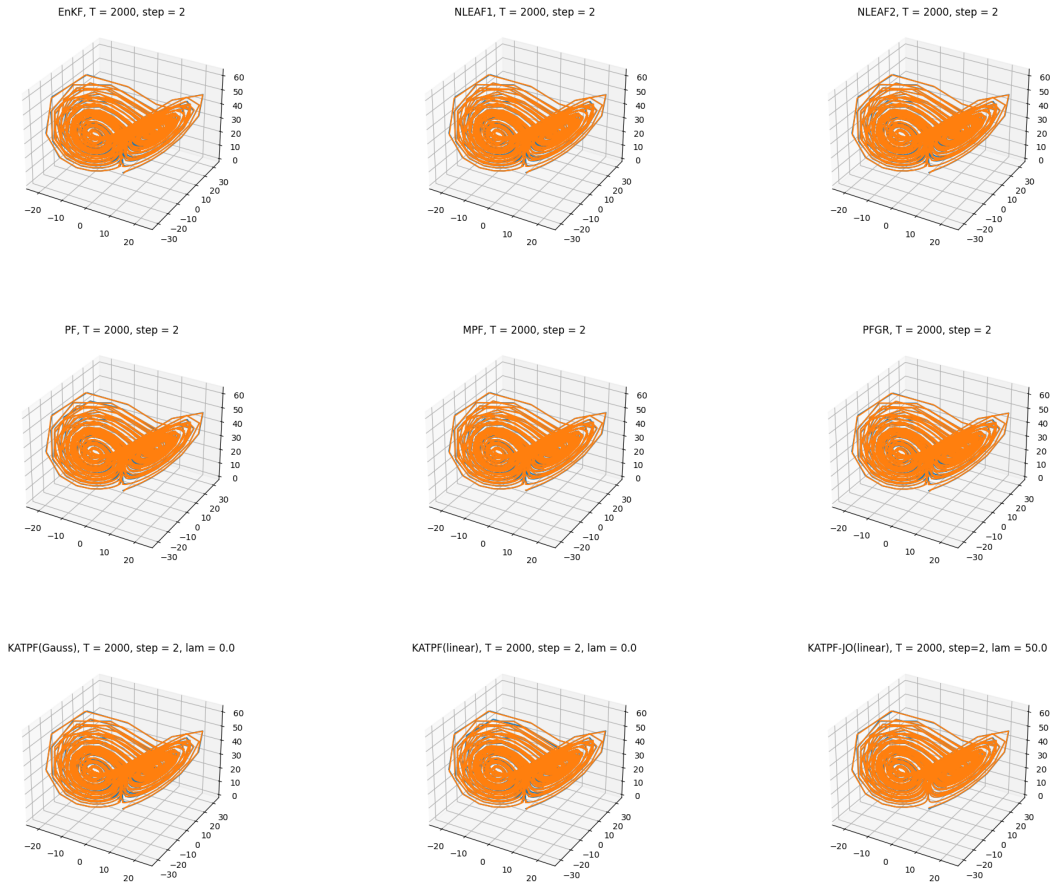


Figure 6: Experimental results of the Lorenz63 system when $T = 2000$ and $\Delta t = 0.04$.

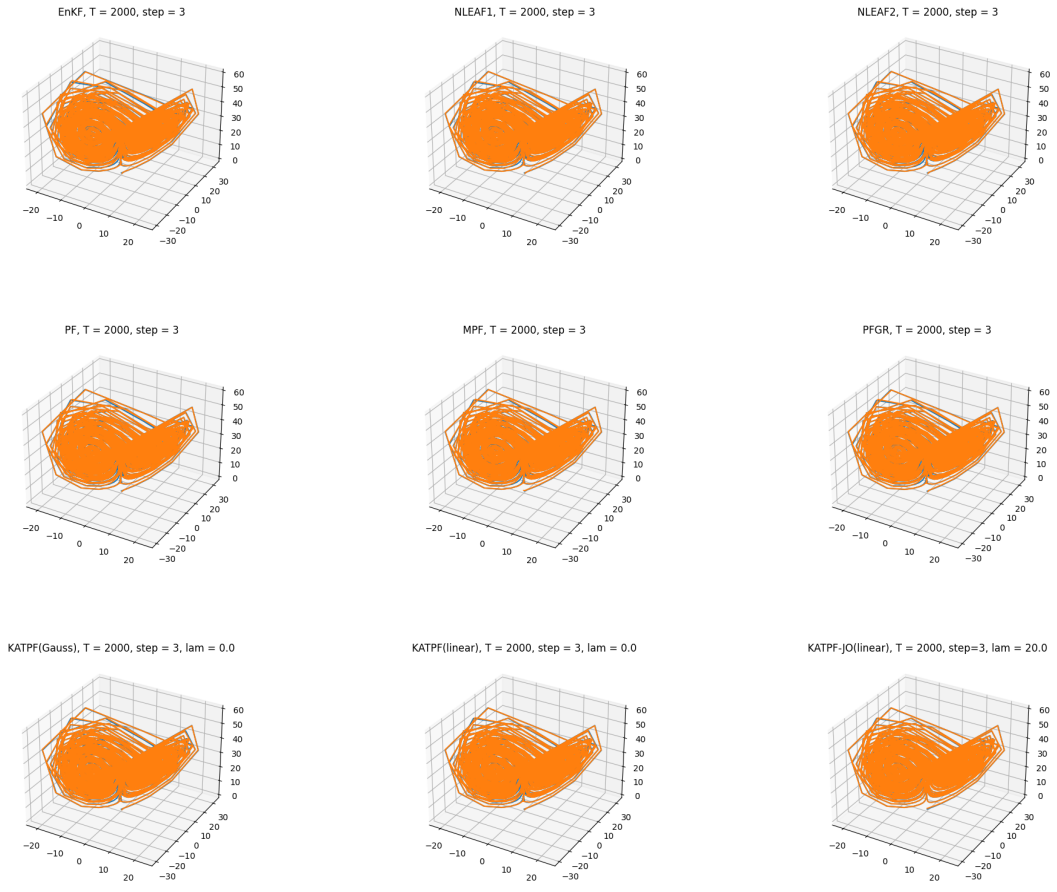


Figure 7: Experimental results of the Lorenz63 system when $T = 2000$ and $\Delta t = 0.06$.

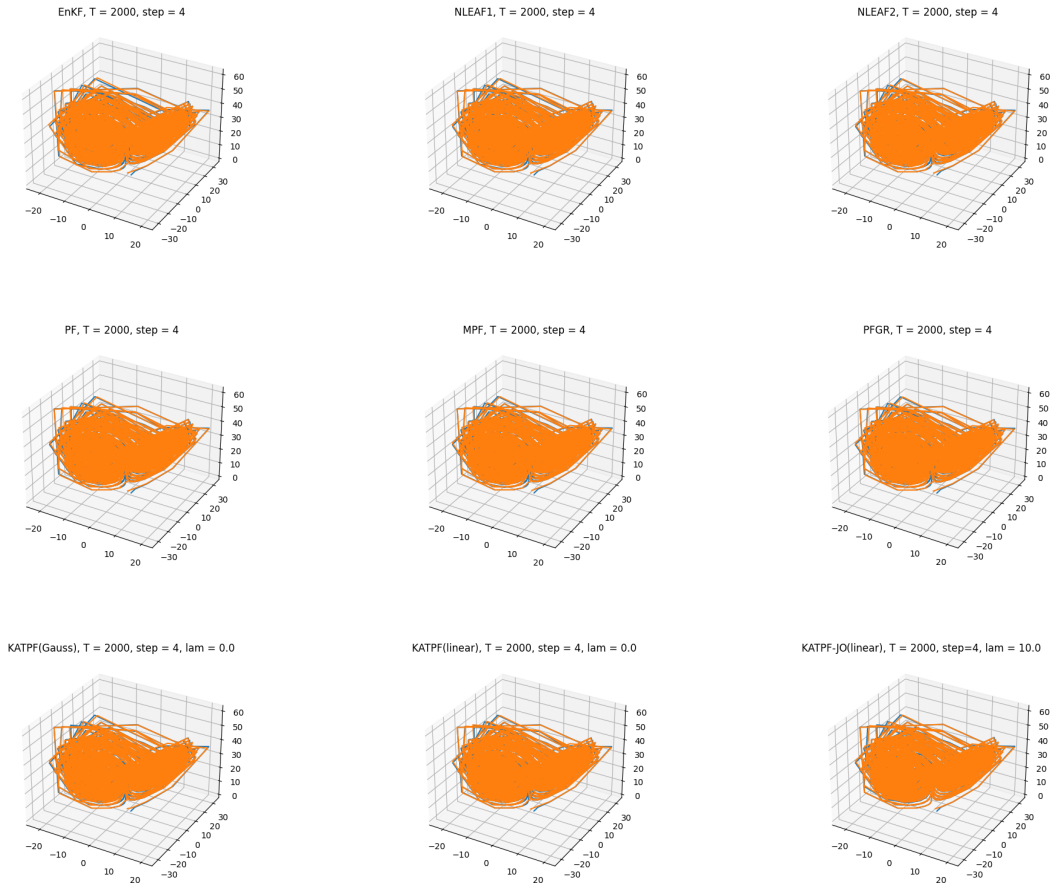


Figure 8: Experimental results of the Lorenz63 system when $T = 2000$ and $\Delta t = 0.08$.

Table 4: Supplementary experimental results (RMSE) of the Lorenz63 system for ablation study. “↗”: the algorithmic convergence becomes worse and accordingly RMSE increases.

KATPF-JO(linear)	$\lambda = 0$	$\lambda = 1$	$\lambda = 10$	$\lambda = 20$	$\lambda = 50$	λ^*
$T = 100, \Delta t = 0.02$	0.1836	0.1652	0.1621	0.1582	0.1445	0.1398
$T = 2000, \Delta t = 0.02$	0.1441	0.1335	0.1143	0.1068	0.0965	0.0843
$T = 2000, \Delta t = 0.04$	0.1819	0.1641	0.1380	0.1277	0.1157	0.1157
$T = 2000, \Delta t = 0.06$	0.1767	0.1412	0.1142	0.0973	↗	0.0973
$T = 2000, \Delta t = 0.08$	0.2130	0.1795	0.1305	↗	↗	0.1305

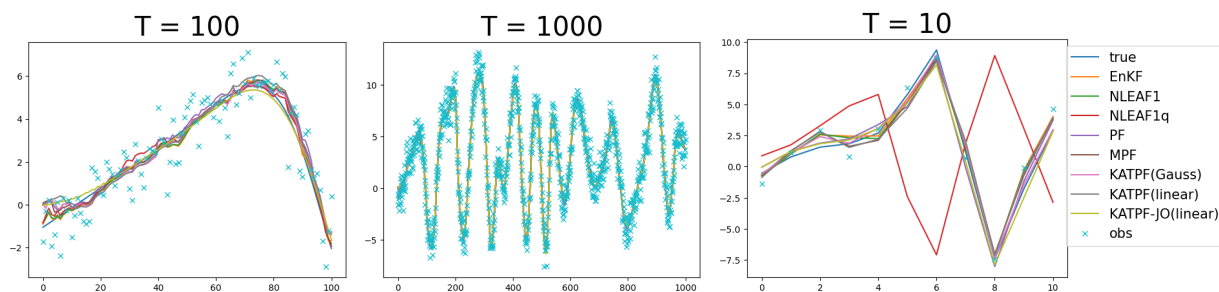


Figure 9: State at location 1 over time in the Lorenz96 system.

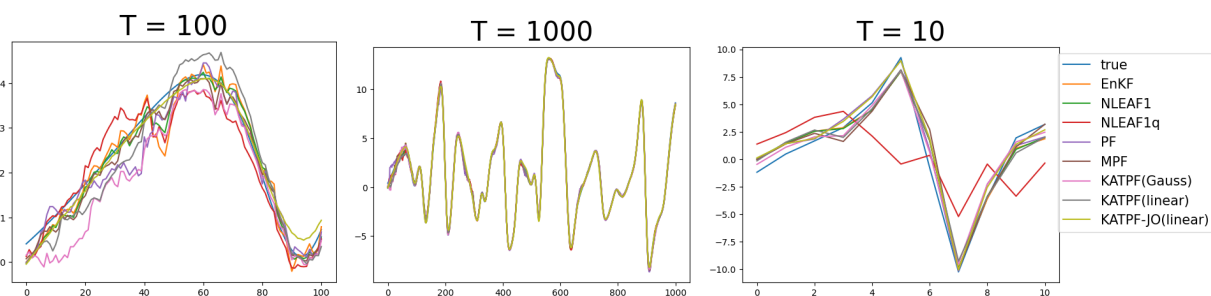


Figure 10: State at location 2 over time in the Lorenz96 system (Recall that observation of this location is missing).

C Covariance Inflation, Localization and Covariance Tapering

In practice, covariance inflation (Lei & Bickel, 2011), localization (Hunt et al., 2007) and covariance tapering (Furrer et al., 2006) are all commonly used to adapt the ensemble methods to the high-dimensional scenarios.

Covariance inflation is usually executed after the analysis step but before the forecast step, where the particles are adjusted as follows:

$$x_t^i \leftarrow \bar{x}_t + (1 + \delta)(x_t^i - \bar{x}_t) \quad (43)$$

with some $\delta > 0$. Lei & Bickel (2011) used slightly different inflation method for PF:

$$x_t^i \leftarrow x_t^i + 2\delta \text{Cov}(x_t)^{\frac{1}{2}} \xi_t^i \quad (44)$$

with $\xi_t^i \stackrel{\text{i.i.d.}}{\sim} \mathcal{N}(0, 1)$. This can also be interpreted as a form of the regularized PF described in Section 1 and Section 2.2, with the Gaussian kernel. Following Lei & Bickel (2011), unless otherwise specified, we use equation 44 for PFs and equation 43 for other methods after each analysis step in our experiments.

In the localization method, the overall state $x_t = (x_{t,1}, \dots, x_{t,d})$ is divided into d overlapping sub-states $\{x_{t,N_j}\}_{j=1}^d$ with $x_{t,N_j} = (x_{t,j-l}, \dots, x_{t,j}, \dots, x_{t,j+l})$ for some positive integer $l \leq \frac{d-1}{2}$ (with all indices taken modulo d). Each sub-state x_{t,N_j} is updated using its corresponding sub-observation $y_{t,\tilde{N}_j} := H_t|_{N_j} x_{t,N_j}$ ($H_t|_{N_j}$ means the restriction of H_t to the coordinate set N_j). Therefore, each coordinate $x_{t,j}$ is updated simultaneously in $2l + 1$ sub-states $x_{t,N_{j-l}}, \dots, x_{t,N_j}, \dots, x_{t,N_{j+l}}$. The final update for $x_{t,j}$ is obtained by averaging the updates derived across the $2k + 1$ sub-states $x_{t,N_{j-k}}, \dots, x_{t,N_j}, \dots, x_{t,N_{j+k}}$, where $k \leq l$.

The fundamental idea behind covariance tapering is to sparsify the covariance matrix by introducing zeros deliberately. Let T_θ be a sparse positive definite correlation matrix (e.g., Katzfuss et al. (2016); Furrer et al. (2006)). Then the tapered covariance is computed as an element-wise product:

$$\text{Cov}_{\text{tap}}(x, x') = \text{Cov}(x, x') \odot T_\theta(x, x'). \quad (45)$$

We can use $\widehat{\text{Cov}}_{\text{tap}}(x, x')$ instead of the sample covariance $\widehat{\text{Cov}}(x, x')$ to estimate the population covariance. It is important to note that this technique is applicable and practical only for filtering methods that require covariance estimation, such as the EnKF.